Coseismic slip on the southern Cascadia megathrust implied by tsunami deposits in an Oregon lake and earthquake-triggered marine turbidites

Robert C. Witter,[1,2] Yinglong Zhang,[3] Kelin Wang,[4] Chris Goldfinger,[5] George R. Priest,[1] and Jonathan C. Allan[1]

Received 26 April 2012; revised 24 August 2012; accepted 29 August 2012; published 9 October 2012.

[1] We test hypothetical tsunami scenarios against a 4,600-year record of sandy deposits in a southern Oregon coastal lake that offer minimum inundation limits for prehistoric Cascadia tsunamis. Tsunami simulations constrain coseismic slip estimates for the southern Cascadia megathrust and contrast with slip deficits implied by earthquake recurrence intervals from turbidite paleoseismology. We model the tsunamigenic seafloor deformation using a three-dimensional elastic dislocation model and test three Cascadia earthquake rupture scenarios: slip partitioned to a splay fault; slip distributed symmetrically on the megathrust; and slip skewed seaward. Numerical tsunami simulations use the hydrodynamic finite element model, SELFE, that solves nonlinear shallow-water wave equations on unstructured grids. Our simulations of the 1700 Cascadia tsunami require >12–13 m of peak slip on the southern Cascadia megathrust offshore southern Oregon. The simulations account for tidal and shoreline variability and must crest the ~6-m-high lake outlet to satisfy geological evidence of inundation. Accumulating this slip deficit requires ≥360–400 years at the plate convergence rate, exceeding the 330-year span of two earthquake cycles preceding 1700. Predecessors of the 1700 earthquake likely involved >8–9 m of coseismic slip accrued over >260 years. Simple slip budgets constrained by tsunami simulations allow an average of 5.2 m of slip per event for 11 additional earthquakes inferred from the southern Cascadia turbidite record. By comparison, slip deficits inferred from time intervals separating earthquake-triggered turbidites are poor predictors of coseismic slip because they meet geological constraints for only 4 out of 12 (~33%) Cascadia tsunamis.

Citation: Witter, R. C., Y. Zhang, K. Wang, C. Goldfinger, G. R. Priest, and J. C. Allan (2012), Coseismic slip on the southern Cascadia megathrust implied by tsunami deposits in an Oregon lake and earthquake-triggered marine turbidites, *J. Geophys. Res.*, *117*, B10303, doi:10.1029/2012JB009404.

1. Introduction

[2] Recurrence intervals of great (moment magnitude, $M_w > 8$) earthquakes on the Cascadia megathrust provide key constraints on earthquake size for seismic and tsunami hazard assessments aimed at reducing risk [e.g., *Petersen et al.*, 2008; *González et al.*, 2009; *Priest et al.*, 2009]. The megathrust is the principal fault within the 1,100-km long Cascadia subduction zone where the Juan de Fuca and Gorda plates descend beneath North America at ~40 mm yr^{-1} [*DeMets et al.*, 2010] (Figure 1a). Along the northern part of the Cascadia plate boundary, Late Holocene paleoseismological records of coastal earthquake-induced subsidence and offshore turbidites interpreted to be the consequence of seismic shaking indicate that great earthquakes probably ruptured the megathrust every 500–600 years, on average, with individual intervals between earthquakes varying from a few centuries to about 1,000 years [*Adams*, 1990; *Atwater and Hemphill-Haley*, 1997]. However, newer data from the southern Cascadia margin imply earthquake ruptures that vary in length and have shorter recurrence intervals compared to northern Cascadia [*Clarke and Carver*, 1992; *Kelsey et al.*, 2005; *Nelson et al.*, 2006; *Goldfinger et al.*, 2008, 2012].

[3] The most recent Cascadia earthquake, on 26 January 1700, attained M_w 9 [*Satake et al.*, 1996, 2003]. Numerical simulations of the tsunami generated by the 1700 earthquake that agree with documented tsunami heights in Japan require

[1]Coastal Field Office, Oregon Department of Geology and Mineral Industries, Newport, Oregon, USA.
[2]Now at Alaska Science Center, U.S. Geological Survey, Anchorage, Alaska, USA.
[3]OGI School of Science and Engineering, Oregon Health and Science University, Beaverton, Oregon, USA.
[4]Pacific Geoscience Centre, Geological Survey of Canada, Sidney, British Columbia, Canada.
[5]College of Oceanic and Atmospheric Sciences, Oregon State University, Corvallis, Oregon, USA.

Corresponding author: R. C. Witter, Alaska Science Center, U.S. Geological Survey, Anchorage, AK 99508, USA. (rwitter@usgs.gov)

0148-0227/12/2012JB009404

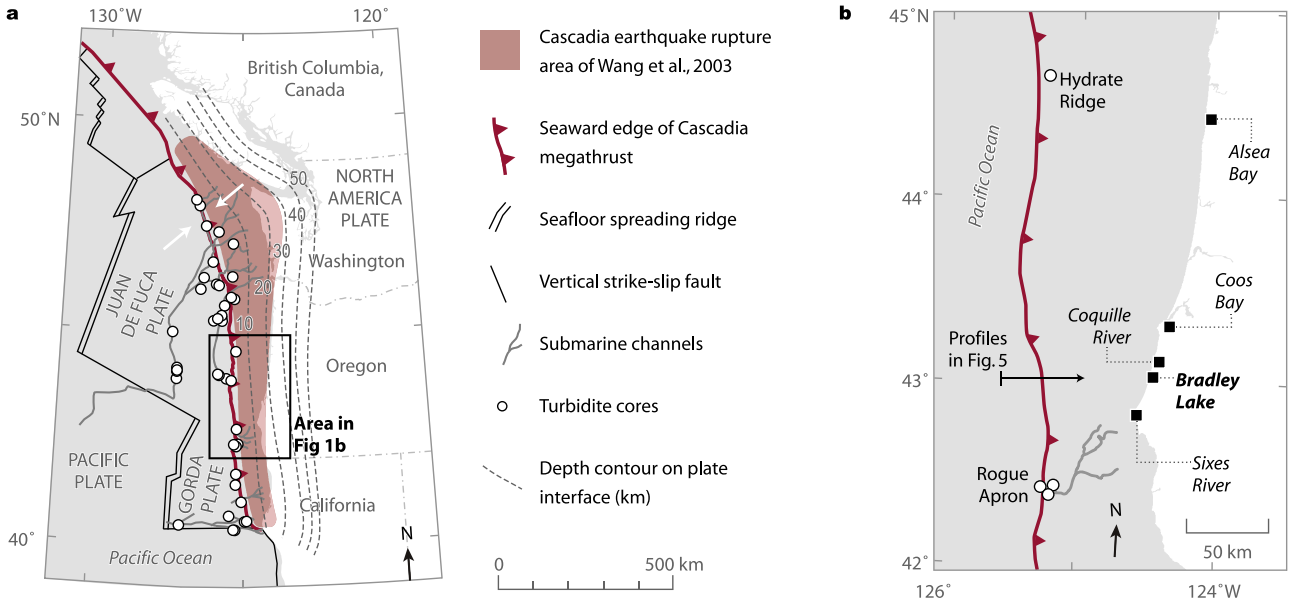

Figure 1. Index maps. (a) Plate-tectonic setting of the northwestern United States. White arrows show plate convergence at 40 mm yr^{-1} [*DeMets et al.*, 2010]. (b) Map of southern Oregon coast showing deep sea core sites (white circles) containing offshore turbidites studied by *Goldfinger et al.* [2012]. Squares mark onshore sites harboring geological evidence of coastal subsidence and tsunami inundation. Possible correlations among paleoseismological records from sites shown on this map are shown in Figure 4.

an earthquake source with 18–21 m of coseismic slip along the entire 1,100-km length of the Cascadia megathrust [*Satake et al.*, 2003]. Other estimate involve <10–50 m of variable slip along the megathrust in 1700, derived from elastic dislocation models guided by tectonic subsidence data compiled for Cascadia coastal sites [*Leonard et al.*, 2004, 2010]. More quantitative estimates of coseismic subsidence at six sites along the Oregon coast imply megathrust slip that varied between 10 and 30 m, consistent with a M_w 9 earthquake [*Hawkes et al.*, 2011]. However, considerable uncertainty in subsidence estimates in southern Oregon and northern California leaves inferred amounts of slip there an open question. Do shorter recurrence intervals of earthquake-triggered turbidites in southern Cascadia (220–380 years on average [*Goldfinger et al.*, 2012] imply a history of more frequent plate-boundary earthquakes with commensurably less amounts of coseismic slip?

[4] In southern Cascadia, discrepancies between offshore and onshore earthquake records suggest that predecessors of the 1700 earthquake varied in size and imply that amounts of fault slip varied during ruptures on megathrust segments of different length [*Kelsey et al.*, 2002; *Witter et al.*, 2003; *Nelson et al.*, 2006; *Goldfinger et al.*, 2012]. For example, in the past 4,600 years, 12 tsunamis deposited sand in Bradley Lake on the southern Oregon coast [*Kelsey et al.*, 2005]. However, only 8–10 earthquakes had sufficient slip on the part of the megathrust below Bradley Lake to subside adjacent estuaries by 0.5 m or more [*Kelsey et al.*, 2002; *Witter et al.*, 2003]. To explain these discrepancies, *Nelson et al.* [2006] reasoned that some Cascadia tsunamis recorded in Bradley Lake may have attended magnitude-8 earthquakes that produced too little subsidence to leave stratigraphic evidence in nearby salt marshes. In contrast, 23 offshore turbidites deposited in Rogue Apron over the same time period have been interpreted by *Goldfinger et al.* [2012] to reflect strong shaking during megathrust earthquakes. Whether the turbidites that lack onshore correlatives—often thin, mud turbidites present only along the southern Cascadia margin [*Goldfinger et al.*, 2012]—record megathrust seismicity or some other process remains a subject of some debate [*Frankel*, 2011; *Atwater and Griggs*, 2012].

[5] In this paper we estimate coseismic slip on the southern Cascadia megathrust using numerical tsunami simulations and prehistoric tsunami deposits in Bradley Lake. First, we examine discrepancies in southern Cascadia paleoseismological records, including onshore and offshore data, between the latitudes of Hydrate Ridge and Rogue Apron (Figure 1b). Second, we reconstruct plausible, hypothetical coastal landscapes and shoreline configurations likely encountered by prehistoric Cascadia tsunamis. Third, we use a three-dimensional fault dislocation model (modified from *Priest et al.* [2009]) to compute seafloor deformation for tsunami sources. Fourth, we numerically simulate tsunami inundation at Bradley Lake to estimate the minimum megathrust slip required to generate waves that reach the outlet elevation of the lake. Finally, we use the results to construct a simple slip budget spanning 12 hypothetical earthquake cycles and compare it to slip deficits implied by recurrence intervals of southern Cascadia turbidites. Differences between these independent estimates of slip imply that if thin, mud turbidites in southern Cascadia record megathrust ruptures in addition to events evident in the Bradley Lake tsunami record, then the earthquakes that triggered the smaller turbidity currents were

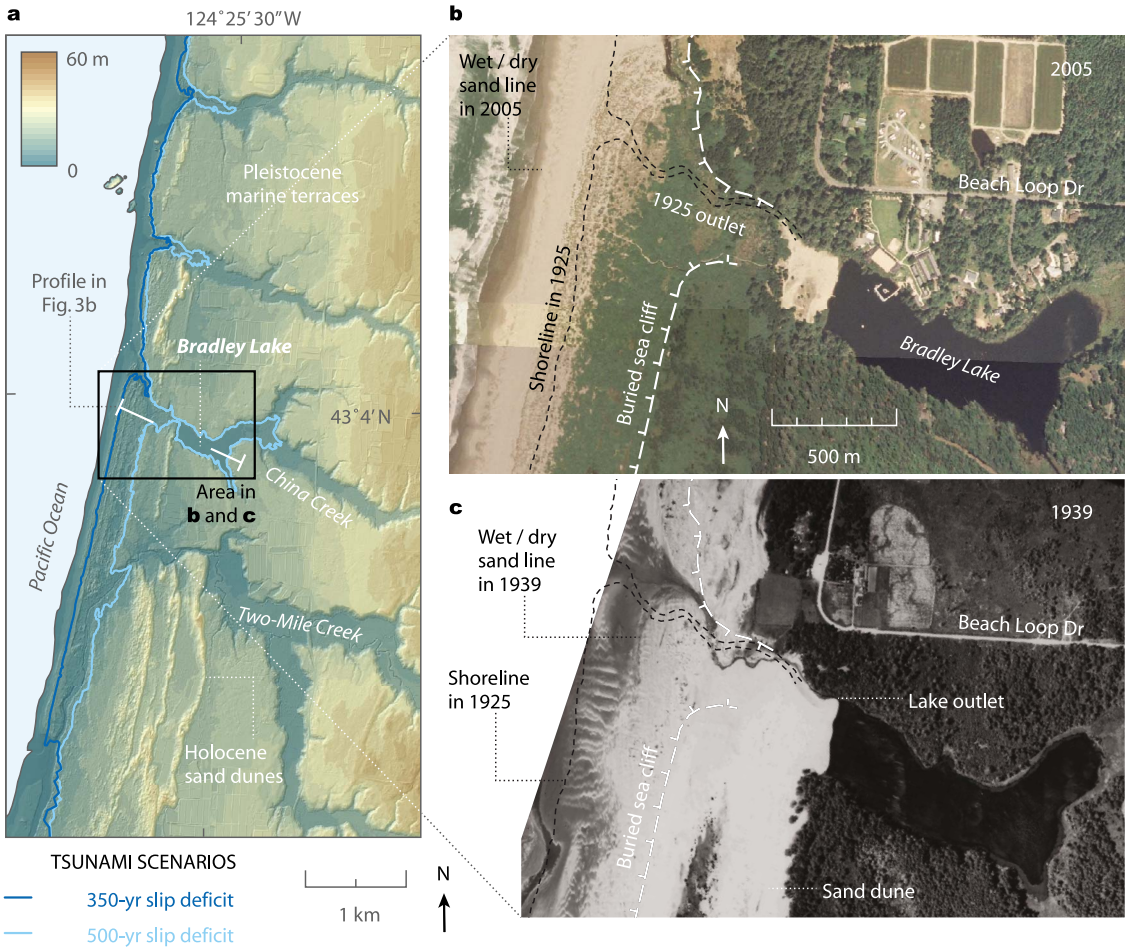

Figure 2. (a) Holocene sand dunes ornament broad Pleistocene marine terraces along the coast near Bradley Lake in southern Oregon (located in Figure 1b). Blue lines show landward limit of simulated tsunami inundation using a model grid with historical topography (Grid A, Figure 6). The lines depict inundation using earthquake scenarios with 11 and 16 m of fault slip, equivalent to 350 years (dark blue) and 500 years (light blue) of plate convergence, respectively. (b) Evidence for recent seaward shift in shoreline position includes a wave eroded sea cliff mantled by dune sand and the shoreline in 1925 mapped by early coastal surveyors [*Bernstein*, 1925] compared to the wet/dry sand line in the 2005 orthophoto. (c) The shoreline probably reached its most landward position in 1939 when winter storms lowered the beach and shifted the shoreline landward of its position in 1925.

likely $M_w < 8.4$ and their tsunamis, if generated, were probably too small to inundate Bradley Lake.

2. Paleoseismological Records of Great Cascadia Earthquakes and Tsunamis in Southern Oregon

[6] Cascadia paleoseismological records have been documented at several coastal sites in southern Oregon, including Coos Bay [*Nelson et al.*, 1996, 1998], Coquille River Estuary [*Witter et al.*, 2003], Bradley Lake [*Kelsey et al.*, 2005], and the Sixes River [*Kelsey et al.*, 2002] at Cape Blanco (Figure 1b). Offshore southern Oregon, paleoseismological records come from stacked turbidites at two sites: Hydrate Ridge and Rogue Apron [*Goldfinger et al.*, 2012].

2.1. Southern Oregon Estuaries

[7] Sharp contacts between buried wetland soils and overlying intertidal mud beneath lowlands fringing estuaries in southern Oregon have been interpreted to reflect episodes of sudden subsidence caused by great Cascadia earthquakes. At some sites, sandy deposits sandwiched between mud and peat have been attributed to tsunamis generated by tectonic deformation offshore.

[8] At Coos Bay, Oregon (Figure 1b), salt marshes along South Slough archive evidence for ten rapid rises in relative sea level in the past ~4,600 years, but only three satisfy enough criteria to support earthquake-induced subsidence as the cause of submergence [*Nelson et al.*, 1996; 1998]. Equivocal evidence for the other seven sharp contacts cannot distinguish between alternative nonseismic explanations and an earthquake origin.

[9] Evidence at the Coquille River estuary (Figure 1b) suggests that 12 Cascadia earthquakes in the past 6,700 years dropped salt marsh and forest soils to tidal flat elevations [*Witter et al.*, 2003]. Sandy sediment inferred to record tsunami inundation overlies all but one of the soils. The average

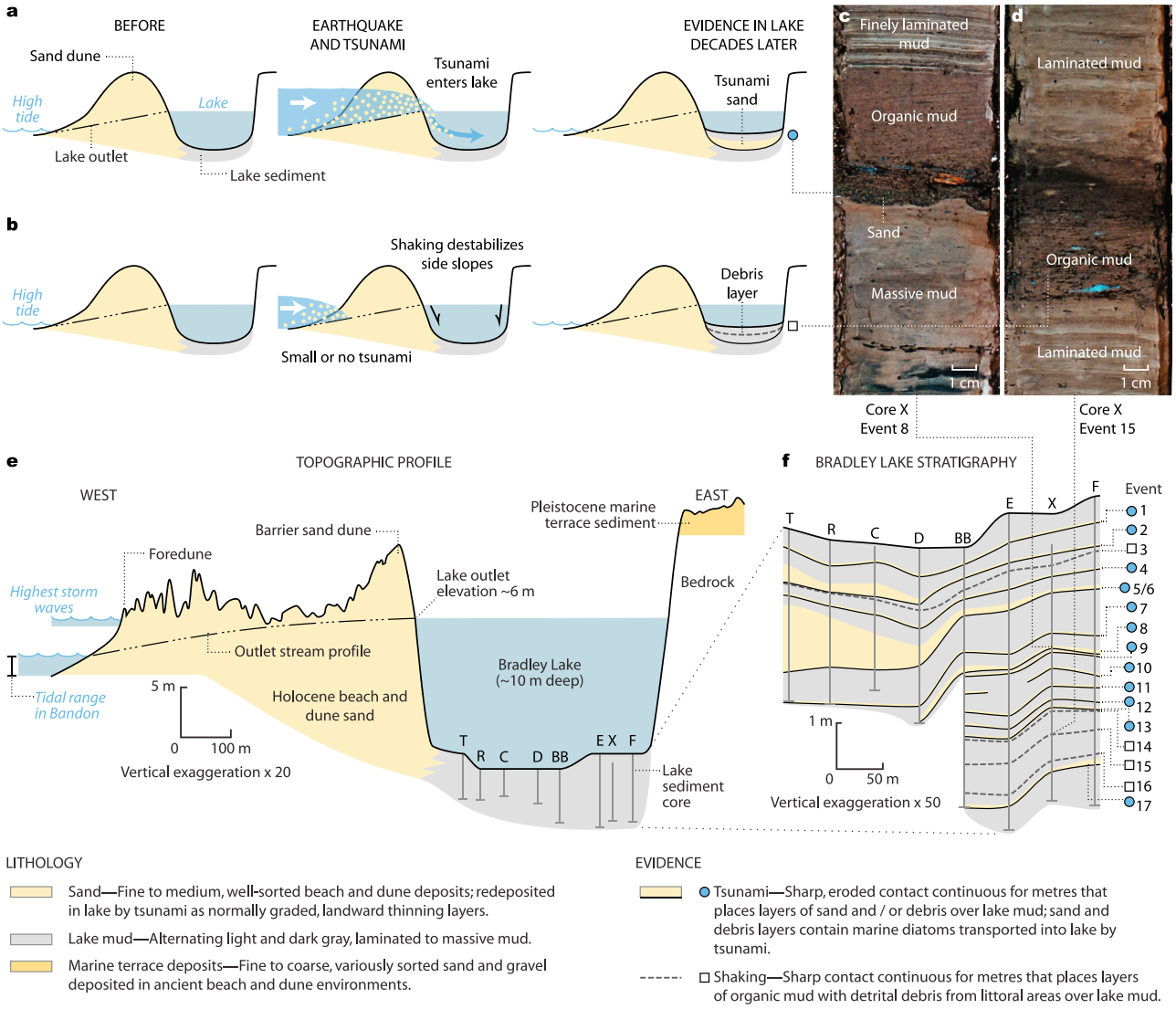

Figure 3. Stratigraphic evidence of disturbances in Bradley Lake sedimentary record caused by great Cascadia earthquakes and their tsunamis [*Kelsey et al.*, 2005]. (a) Conceptual model of tsunami inundation in a coastal lake that leaves a sand deposit in the sedimentary record. (b) Debris layers lacking evidence for tsunami inundation consist of organic mud that interrupts normal laminated lake mud and are inferred to reflect earthquake shaking that destabilizes basin walls. (c) Photo showing sand deposit interpreted to reflect tsunami inundation. (d) Photo showing organic mud layer inferred to reflect seismic shaking. (e) Topographic profile of coast between the Pacific Ocean and Bradley Lake. (f) Stratigraphic profile of Bradley Lake sediment. Blue circles denote evidence for tsunami inundation. White squares denote evidence for strong shaking without tsunami overtopping the lake outlet.

interval between events at the Coquille River is 570–590 years, but varies from a few hundred years to over 1,000.

[10] The lower Sixes River valley near Cape Blanco (Figure 1b) preserves stratigraphic evidence of 11 ruptures of the plate boundary over the past 5,500 years that abruptly lowered wetland soils into the intertidal zone [*Kelsey et al.*, 2002]. Earthquakes recorded at the Sixes River occurred on average every 510 years and were accompanied by tsunamis and, on at least two occasions, strong shaking that liquefied sandy sediments. The Sixes River earthquake chronology, along with observations from the Coquille River estuary, provided some of the first supporting evidence for the hypothesis that not all Cascadia earthquakes ruptured the entire length of the subduction zone [*Kelsey et al.*, 2002; *Witter et al.*, 2003].

2.2. Bradley Lake

[11] Bradley Lake's proximity to the Pacific Ocean and its position above the Cascadia megathrust made it a natural tsunami gauge about 7,500 years ago when landward-advancing sand dunes barred China Creek (Figure 2). Distinctive and unusual disturbances that interrupt laminated lacustrine mud reflect seismic shaking and tsunami inundation caused by 17 prehistoric Cascadia earthquakes [*Kelsey et al.*, 2005] (Figure 3). In 13 cases the disturbances record sustained surges of ocean water that blanketed the lake floor

with landward-thinning sheets of sand carried from nearshore, beach and dune environments. *Kelsey et al.* [2005] reasoned that over the period when the lake was an optimal tsunami recorder (~4,600 years ago to the present) its elevation (~6 m NAVD 88) was too high to be breached by distant tsunamis generated by plate-boundary ruptures around the Pacific Ocean.

[12] Other processes, like short-period waves (tens of seconds) driven by north Pacific storms offered less likely explanations for the disturbances. For justification, *Kelsey et al.* [2005] (Figure 3) pointed to short-lived peaks in lake salinity, evident from Holocene marine diatoms present in disturbed sediments, that required marine water to flow into the lake for tens of minutes to hours—conditions best explained by Cascadia tsunamis, including the most recent waves in 1700.

2.3. The Offshore Turbidite Record

[13] Shaking during at least 13 great earthquakes since the eruption of Mount Mazama (~7.6 ka) triggered turbidity currents in multiple submarine canyon heads along the Cascadia margin that deposited rhythmic beds of sand and silt in the floors of offshore channels and abyssal fans [*Adams*, 1990]. Decades after they were first described by *Griggs and Kulm* [1970], *Adams* [1990] proposed that these turbidite deposits required synchronous triggering by regional earthquakes for two reasons. First, following *Pilkey*'s [1988] study of turbidites in the Mediterranean Sea and Puerto Rico Trench, Adams argued that the same number of turbidites above and below channel confluences indicate a phenomenon of regional triggering, so that local mechanisms like shallow crustal earthquakes (e.g., M 6.5 within 50 km of a canyon head) or self-triggering at multiple canyon heads with different sediment loading rates could be ruled out. He further reasoned that the coincidence of 13 turbidites at multiple sites spanning 580 km, from Rogue Apron in the south to Cascadia Channel in the north, was most simply explained by a series of great earthquakes. Turbidite studies along other tectonically active margins have expanded on *Adams*'s [1990] approach and show that sedimentological attributes and tests for synchronous triggering can distinguish turbidites triggered by earthquakes versus other processes [e.g., *Gorsline et al.*, 2000; *Nakajima and Kanai*, 2000; *Gràcia et al.*, 2010; *Goldfinger et al.*, 2008].

[14] A reexamination of the southern Cascadia turbidite record by *Goldfinger et al.* [2008, 2012] implies shorter earthquake recurrence times (220–380 years on average) along the southern margin compared to the 500–530 year average recurrence times for turbidites that correlate along the entire Cascadia margin. Turbidites offshore southern Oregon include sequences deposited in a 10-km long, slope basin west of Hydrate Ridge, a structural high in the accretionary wedge, and stacked deposits within a 2-km wide apron at the base of Rogue Canyon, ~250 km to the south (Figure 1b). Subtle features of the Hydrate and Rogue cores include dark intervals with silty bases—distinct from the pelagic clay—that thicken sections between sandy turbidites correlated along the entire margin. These so-called "mud turbidites" account for 11 of 24 turbidites at Hydrate Ridge and 19 of 32 turbidites at Rogue Apron, deposited since 7.5 ka (Figure 4) [*Goldfinger et al.*, 2012].

[15] Hydrate Ridge's western basin is encircled on three sides by high, structural ridges that block sediment delivery from sources outside the basin, limiting sources to the high ridges directly adjacent to the basin. This isolation and the absence of Mazama ash in cores at Hydrate Ridge eliminates storms, tsunamis, hyperpycnal flows (density currents during high discharge river floods), and other shallow water processes as sources of turbidity currents. Other processes like slope destabilization by gas hydrates or local slumping are unlikely causes of turbidites at Hydrate Ridge because of the fidelity of stratigraphic correlations with cores from Rogue Apron, the consistency among radiocarbon age estimates, and the agreement between offshore and onshore earthquake evidence [*Goldfinger et al.*, 2012]. Additional turbidites observed in cores south of the Trinidad system may have been triggered by processes other than megathrust seismicity [*Goldfinger et al.*, 2012]. Turbidites offshore northern California may be more numerous because of the higher rate of shallow crustal earthquakes and a narrower shelf that brings offshore canyon heads closer to sediment-laden river systems, increasing the susceptibility to storm-driven turbidity currents. Refer to *Goldfinger et al.* [2012] for a comprehensive discussion of alternative turbidite triggering mechanisms.

3. Correlation of Paleoseismological Records

[16] We correlate the Bradley Lake chronology of Cascadia tsunamis with the most reliable evidence of great earthquakes from nearby Oregon estuaries and with a chronology of more frequent earthquakes along the southern plate-boundary inferred from turbidite records at Hydrate Ridge and Rogue Apron [*Goldfinger et al.*, 2012]. Correlations (Figure 4) consider three aspects of published data for the various earthquake records: (1) physical properties of

Figure 4. Correlation of radiocarbon data from coastal paleoseismic sites in south-central Oregon and offshore turbidite sequences from Hydrate Ridge and Rogue Channel. Stratigraphic correlations of turbidites have been interpreted by *Goldfinger et al.* [2012] to reflect long (>500 km) fault ruptures (bold dashes) of most of the megathrust from shorter (<500 km) fault segment breaks (thin dashes) along the southern margin. Up arrows denote maximum age estimates on detrital samples. Symbol width represents relative size of earthquake inferred from deposit thickness or amount of subsidence evident in change in microfossil assemblages. Rectangles represent inferred earthquake age ranges in calendar years before 1950, calibrated from radiocarbon dates using Calib 5.0.2 software [*Stuiver and Reimer*, 1993; M. Stuiver, P. J. Reimer, and R. W. Reimer, CALIB 5.0, 2005, available at http://calib.qub.ac.uk/calib/], the calibration database of *Reimer et al.* [2004] and the marine reservoir database of *Hughen et al.* [2004]. The age ranges presented here have been recalibrated from the original laboratory reported age and are compiled in *Goldfinger et al.* [2012, Appendix 1]. Original age data for Cascadia earthquake records from coastal sites are reported in studies at Alsea Bay [*Nelson et al.*, 2008]; Coos Bay [*Nelson et al.*, 1996, 1998]; Coquille River [*Witter et al.*, 2003]; Bradley Lake [*Kelsey et al.*, 2005]; and Sixes River [*Kelsey et al.*, 2002].

turbidites that strengthen stratigraphic correlations along the Cascadia margin [*Goldfinger et al.*, 2012]; (2) the agreement (overlap) of 2σ calibrated radiocarbon age ranges; and (3) qualitative estimates of earthquake size depicted by the widths of symbols in Figure 4 [e.g., *Nelson et al.*, 2006; *Goldfinger et al.*, 2012]. For example, thick dashed lines in Figure 4 designate stratigraphic correlations of the longest ruptures inferred by matching characteristic sedimentary signatures in grain size distribution, sediment density, and magnetic susceptibility of turbidites within the same channel and between different channel systems separated by hundreds of kilometers [*Goldfinger et al.* 2012]. Stratigraphic correlations of thinner, mud turbidites (thin dashed lines in Figure 4) with shared physical properties from cores along the southern margin may reflect shorter ruptures.

[17] Symbology in Figure 4 also designates relative size inferred for each earthquake. Relative sizes of turbidite beds are considered to generally represent relative sizes of

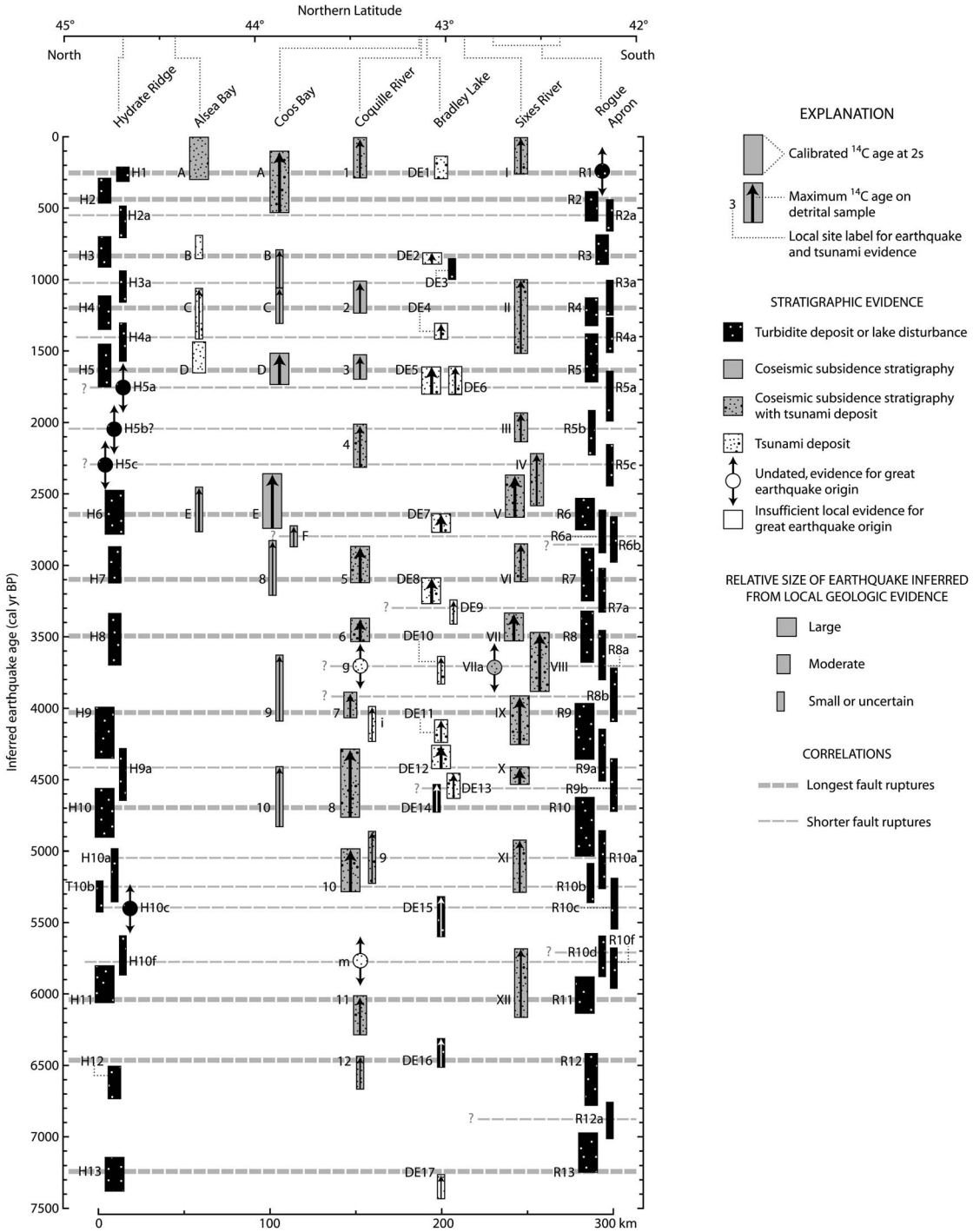

Figure 4

earthquakes, an inference supported by the observed consistency of the correlated turbidite beds along strike. This topic and estimated rupture lengths and relative magnitudes are discussed further in *Goldfinger et al.* [2012]. Relative sizes of earthquakes inferred from evidence at Bradley Lake, Alsea Bay and Coos Bay come from *Nelson et al.* [2006]. The relative sizes of earthquakes recorded at the Coquille and Sixes River estuaries in southern Oregon are inferred from estimates of coseismic subsidence, lateral extent of submergence and thickness of tsunami deposits [*Kelsey et al.*, 2002; *Witter et al.*, 2003].

[18] Confidence in the correlations are limited by 2σ age ranges spanning 200–300 calendar years, which in many cases leaves open more than one possible alternative [e.g., *Nelson et al.*, 2006]. The radiocarbon age ranges plotted in Figure 4 are compiled by *Goldfinger et al.* [2012, Appendix 1]. The ^{14}C dates from original studies were calibrated using Calib 5.0.2 software [*Stuiver and Reimer*, 1993; M. Stuiver, P. J. Reimer, and R. W. Reimer, CALIB 5.0, 2005, available at http://calib.qub.ac.uk/calib/], the calibration database of *Reimer et al.* [2004] and the marine reservoir database of *Hughen et al.* [2004]. If any of the earthquake records include events separated by a few decades, like historical examples from Nankai trough [*Ando*, 1975], Alaska, Columbia [*Thatcher*, 1990] and the Sunda megathrust [*Briggs et al.*, 2006], then we cannot differentiate them. Further uncertainty in the age estimates comes from the indefinite relation between the material dated and the time of the earthquake.

[19] Ages for land records mostly come from detrital plant macrofossils, whereas turbidite ages reflect analyses of marine foraminifera and require marine reservoir correction [*Hughen et al.*, 2004; *Goldfinger et al.*, 2012]. In almost all cases the sample dated provides a maximum constraint on the time of the earthquake. Bradley ages, though narrower in 2σ range than others, appear to be systematically older when compared to other data, probably because the water-logged needles, moss and twigs submitted for dating died several decades or, in some cases, a few centuries before the tsunami swept them into the lake. Despite these caveats, inferences on relative earthquake size for events at Bradley Lake and adjacent estuaries strengthen correlations with the thickest turbidites while highlighting the obvious discrepancy that turbidites along the southern Cascadia margin outnumber earthquakes recorded at coastal sites by nearly two to one over the past 7,500 years (Figure 4).

[20] The giants ($M_w \geq 9$) among Cascadia earthquakes captured in paleoseismic records probably left evidence at multiple sites that strengthen some correlations. Whereas, the merely great ($M_w > 8$) earthquakes or lesser earthquakes may have triggered turbidites offshore but failed to subside coastal sites low enough or propel tsunamis high enough to exceed thresholds necessary to form and preserve geologic evidence [e.g., *McCalpin and Nelson*, 1996; *Nelson et al.*, 2006]. In the past 7,500 years, 13 of 32 (~41%) southern Cascadia earthquakes, inferred from offshore turbidites, appear to have triggered turbidity currents in submarine canyons and generated tsunamis that inundated Bradley Lake (Figure 4). Lake conditions apparently became more sensitive to recording tsunami inundation about 4,600 years ago because since this time 12 of 23 (~52%) earthquakes appear to be coincident in both the turbidite history and lacustrine record of tsunamis. Although the correlations between tsunami deposits in Bradley Lake and the largest turbidites are not precisely constrained by broad age ranges, alternative correlations with thinner turbidites are less compelling and unsupported by the relative event size data.

[21] Although many correlations remain equivocal, the most compelling include the 1700 earthquake and great earthquakes between 800 and 1,060, 1,300–1,420, 1,370–1,630, 2,350–2,620 and 2,960–3,260 calibrated years before 1950 (cal yr BP) (in Figure 4, 2σ age ranges for Bradley Lake DE2, DE4, DE5, DE7 and DE8). Two lesser great earthquakes, probably of smaller magnitude than the 1700 event, raised tsunami waves that entered Bradley Lake between 1,370 and 1,630 and 3,000–3,490 cal yr BP (DE6 and DE9 in Figure 4). These events, recorded as marine incursions in the lake sediments, probably produced less shaking than their giant cousins because they produced thinner turbidites, and generated too little surface displacement to subside adjacent estuaries that flank Bradley Lake to the north and south [*Kelsey et al.*, 2002; *Witter et al.*, 2003]. An earthquake about 930–1,090 cal yr BP (DE3 in Figure 4) probably produced sufficient shaking to release turbidity currents offshore and destabilize side slopes of Bradley Lake (Figure 3) but failed to generate a tsunami high enough to overtop the 6-m-high (NAVD 88) outlet. Correlations of evidence for tsunamis and shaking in lake sediments older than ~3,500 cal yr BP are less clear and complicate matches with individual turbidites.

4. Tsunami Modeling Approach and Methods

4.1. Simulating Cascadia Tsunamis at Bradley Lake

[22] Coastal and marine evidence of prehistoric Cascadia earthquakes imply that large displacements of the seafloor have produced tsunami waves capable of penetrating the outlet of Bradley Lake. Source details of other great subduction zone earthquakes have been evaluated using numerical tsunami modeling guided by the distribution of tsunami deposits [*MacInnes et al.*, 2010; *Satake et al.*, 2008; *Titov et al.*, 2001]. We perform fault dislocation modeling that predicts seafloor deformation as initial conditions for tsunami simulations run with the hydrodynamic code, SELFE [*Zhang and Baptista*, 2008]. Because seafloor displacement, and hence tsunami size, is sensitive to coseismic slip distribution, we developed three slip models (Figure 5). The first slip model distributes slip symmetrically on a buried fault simulating peak slip along the entire length of the megathrust that tapers to zero both up and downdip [e.g., *Wang and He*, 2008; *Priest et al.*, 2009]. The second model diverts slip to a hypothetical, offshore splay fault [e.g., *Priest et al.*, 2009] by truncating the symmetrical slip distribution of the first model at the surface trace of the splay fault (Figure 5b). We tested a third rupture model that skews megathrust slip seaward (Figure 5b), consistent with limited observations of coseismic deformation produced by the 1964 Alaska earthquake [*Freund and Barnett*, 1976], and the evidence for large seaward slips in the 2011 Tohoku earthquake [*Ide et al.*, 2011; *Fujiwara et al.*, 2011]. Individual scenarios used to compute seafloor displacement are based on these three slip models and encompass a range of peak slip values (8–24 m) that correspond to earthquake recurrence intervals—or potential slip deficits—spanning 250–700 years.

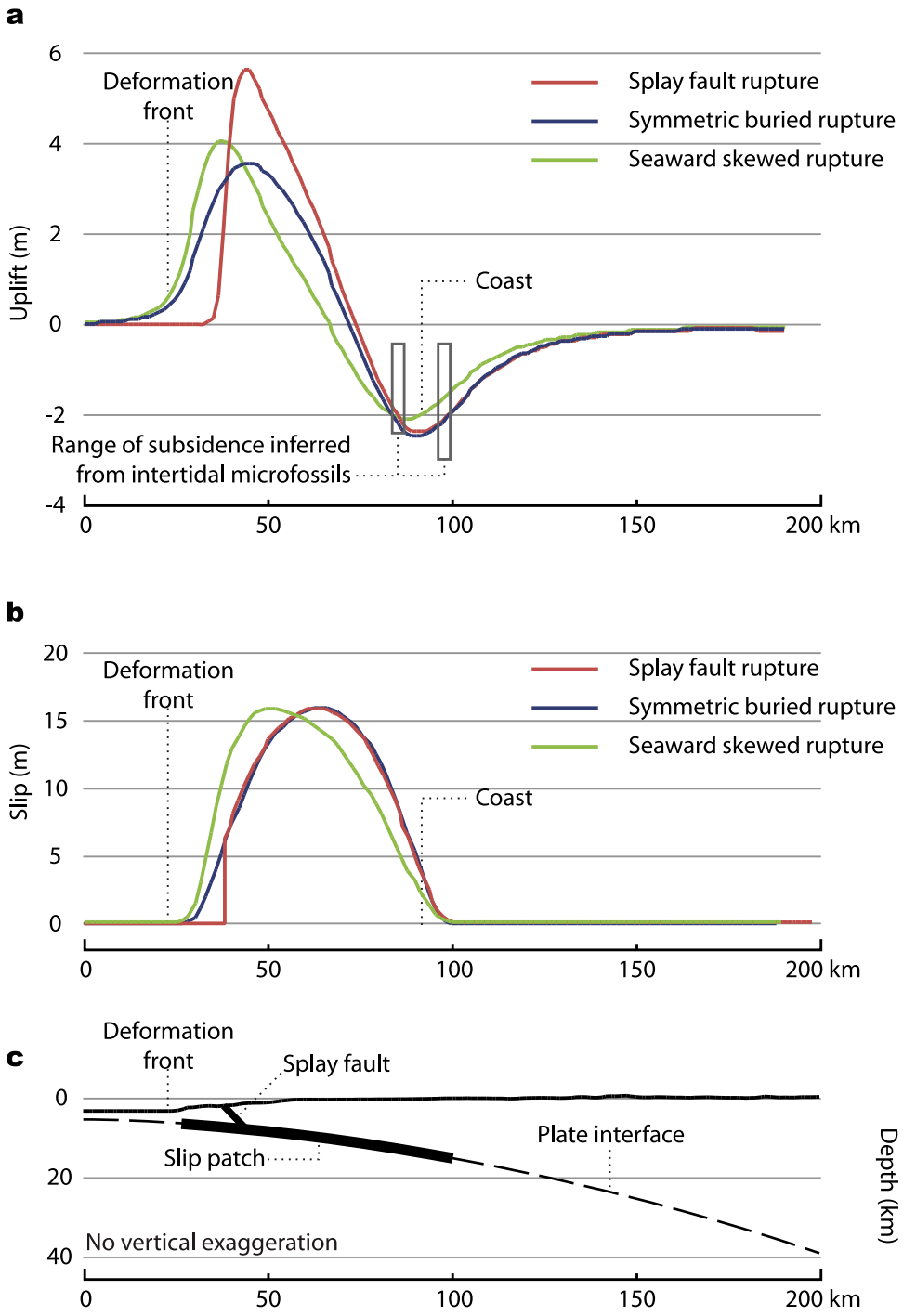

Figure 5. Cascadia earthquake scenarios. (a) Vertical deformation produced by three scenarios at the latitude of Bradley Lake. Rectangles span the range of subsidence inferred from fossil diatom assemblages [*Kelsey et al.*, 2002; *Witter et al.*, 2003]. (b) Profile of fault slip distribution at the latitude of Bradley Lake. Red line shows slip truncated where the splay fault intersects the seafloor. (c) Cross section of the Cascadia subduction zone, at the latitude of Bradley Lake, showing model fault geometry. Bold black line delineates slip patch on plate interface and the geometry of a hypothetical splay fault.

4.2. Summary of Modeling Methods

[23] Surface deformations emulated for earthquake scenarios employ a three-dimensional fault dislocation model [*Okada*, 1985] using a uniform elastic half-space with a Poisson's ratio of 0.25. Slip calculations use Euler vectors that describe the rate and direction of convergence between the Juan de Fuca / Gorda plates and the Cascadia forearc [*Wang et al.*, 2003]. Using this approach, the convergence

rate at the latitude of Bradley Lake is 32 mm yr^{-1}. All fault ruptures use the slip function of *Wang and He* [2008], which was modified from a function proposed by *Freund and Barnett* [1976]. This function allows the slip to decrease in both the updip and downdip directions, reflecting the velocity-strengthening behavior of the shallowest fault segment and the deeper part of the fault. For the shallow end, the behavior of the fault is inferred from limited observations as discussed by *Wang and Hu* [2006]. For the deep end, the fault behavior has been inferred from thermal constraints, stress indicators in the upper plate and agreement between modeled deformation and available paleoseismic estimates of coseismic subsidence [*Kelsey et al.*, 2002; *Witter et al.*, 2003; *Leonard et al.*, 2004, 2010; *Hawkes et al.*, 2011].

[24] Tsunami simulations use the hydrodynamic code, SELFE [*Zhang and Baptista*, 2008]—the Semi-implicit Eulerian-Lagrangian Finite Element model used for cross-scale ocean circulation modeling, tsunamis and storm surges. SELFE solves three-dimensional nonlinear shallow-water wave equations using the finite element method on an unstructured grid. The computational grid has 266,434 nodes and 527,055 triangular elements, with coarser resolution in the open ocean and finer resolution (~5 m) near Bradley Lake. The maximum and minimum grid sizes are about 30 km and 1 m. For simulations in this study the code uses zero values for bottom water friction and viscosity parameters. Algorithms used to solve the Navier-Stokes equations are computationally efficient and stable and have been validated against a number of analytical, laboratory and field-based benchmarks [*Zhang and Baptista*, 2008; *Zhang et al.*, 2011].

4.3. Inferred Late Holocene Evolution of the Coastal Landscape

[25] An evolving late Holocene beach and dune landscape probably influenced overland tsunami flow varying the degree of inundation from one tsunami to the next. Since the early 1900s, Oregon's vast coastal dune sheet has profoundly changed. The introduction of exotic plants (e.g., European beach grass, *Ammophila arenaria*) placed to stabilize sand dunes and prevent encroachment on human development [*Komar*, 1997] has created a modern landscape that was not encountered by prehistoric tsunamis. These changes, evident in historical imagery (Figure 2), have led to a dramatic decrease in the extent of dynamic sand dunes, the construction of densely vegetated, stabilized foredunes that impede marine inundation, and the confinement of a sinuous, north deflected channel of the lake outlet stream.

[26] Paleoseismological data and coastal geomorphology suggest that gradual westward progradation of the shoreline was punctuated by erosion following great earthquakes throughout the late Holocene [e.g., *Meyers et al.*, 1996; *Komar*, 1997]. Our model of the late Holocene landscape evolution west of Bradley Lake places the shoreline closest to the lake where wave erosion formed a sea cliff, now buried by sand dunes but resolved in 2009 LiDAR imagery (Figure 2). This erosion probably occurred shortly after the time Bradley Lake began recording tsunami inundation (~4,600 cal yr BP) [*Kelsey et al.*, 2005]. Since formation of the sea cliff, aeolian sand climbed over and buried the bluff, building a series of foredunes that caused the shoreline to prograde westward. Subsidence accompanying great earthquakes, which is accounted for in tsunami simulations, instantaneously raised sea level by >0.5 m [*Nelson*, 1992; *Kelsey et al.*, 2002; *Witter et al.*, 2003] causing a period of accelerated erosion, first by the tsunami, and then by ocean waves over a period of decades following each event. In between earthquakes, gradual strain accruing on the locked part of the megathrust slowly uplifted the coast [e.g., *Wang et al.*, 2003]. The uplift may have negated slow sea level rise or possibly exposed the beach, promoting further sand accretion and dune mobility. The net response of the sand dune and beach system over multiple earthquake cycles in the late Holocene was gradual westward progradation of the shoreline, interrupted by episodes of erosion following earthquake subsidence, making it increasingly more difficult for tsunamis to inundate the lake [*Kelsey et al.*, 2005].

[27] To examine how late Holocene and historical landscape changes may have influenced tsunami inundation, the simulations use three different unstructured finite element grids depicting hypothetical shorelines that vary in proximity to the lake (Figure 6). As shown on vintage 1939 aerial photography and depicted on U.S. Coast and Geodetic Survey "T-Sheets" from circa 1925 [*Bernstein*, 1925], all grids portray the lake's outlet channel as straighter—and hence more easily flooded by tsunamis—than its present configuration deflected northward by development of recent foredunes (Figure 2). Grid A depicts the straightened outlet channel on modern topography derived from LiDAR collected in 2009. Grid B removes foredunes accentuated by vegetation planted in the 1930s [*Komar*, 1997], shifts the shoreline ~250 m east to near its position in the 1920s, and reflects our best estimate of the shoreline conditions in 1700 (rationale explained in section 5.2). Grid C renders a beach with the shoreline in its most landward position interpreted from the geomorphic expression of a sea cliff buried by Holocene dune sand located ~300 m east of the modern shoreline in grid A (Figures 2 and 6). Grid C was developed as an alternative landscape to examine experimental conditions most favorable to tsunami inundation.

4.4. Variations in Ocean Level

[28] Fluctuations in sea level probably influenced whether tsunamis reached Bradley Lake. Simulations of the most recent Cascadia tsunami assume the waves arrived at or shortly following low tide in the evening of 26 January 1700, according to tidal hindcasts by *Mofjeld et al.* [1997] that include subtidal fluctuations in winter water levels. We also ran additional simulations using mean higher high water (MHHW) to test the model's sensitivity to tide level and, when coupled with grid C, examine hypothetical conditions most favorable for tsunamis to enter the lake (Table 1). We ignore relative sea level change owing to slow vertical strain between earthquakes and late Holocene eustatic sea level rise because such small variations, <0.3 m since 1700 [*Witter et al.*, 2003], fall within decadal variability of climate-related processes controlling ocean levels, like El Niños that elevate winter water levels primarily during the warm phases of the Pacific Decadal Oscillation [*Komar et al.*, 2011].

5. Results

[29] Three models of coseismic slip (Table 1) give rise to a variety of tsunami scenarios, using different shoreline

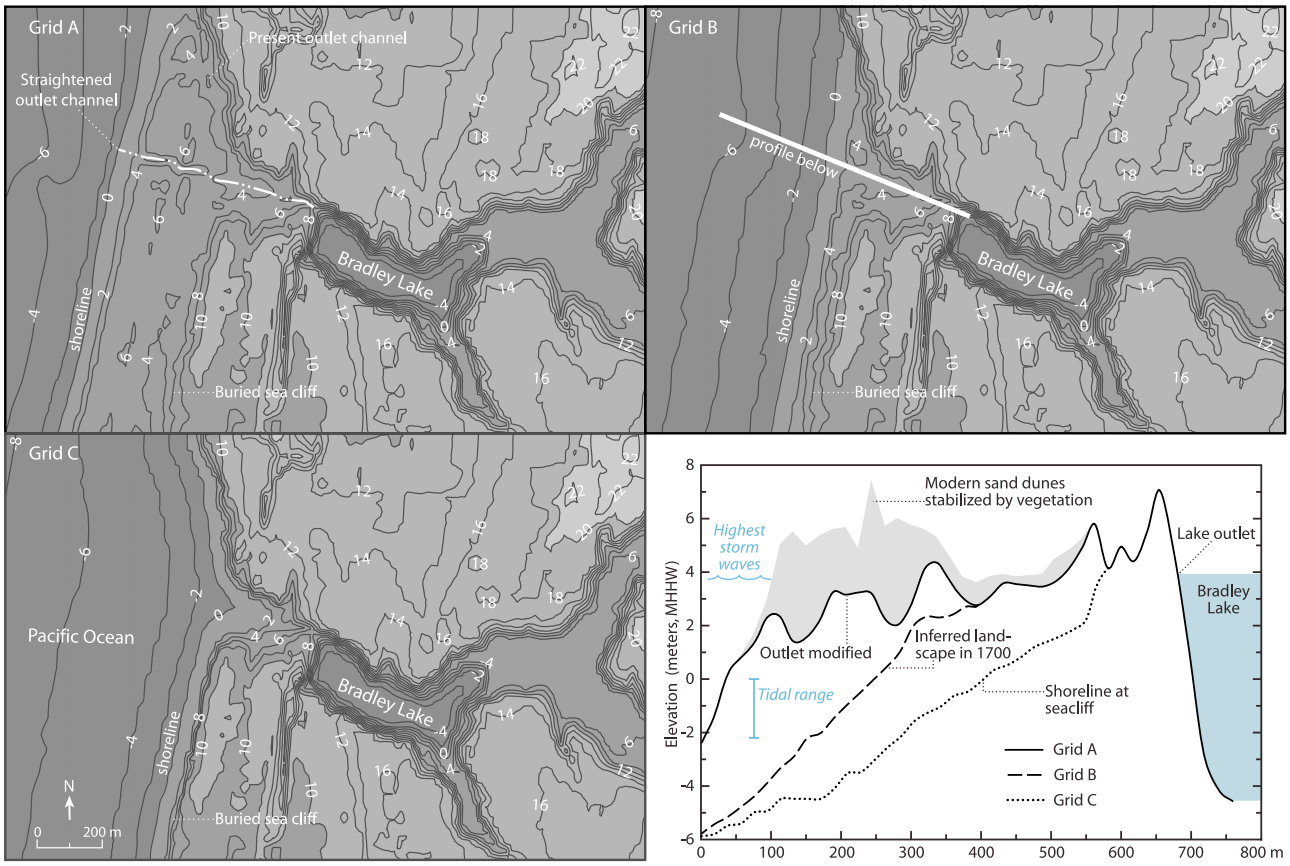

Figure 6. Maps and profiles of numerical grids used in tsunami simulations referenced to the mean higher high water tidal datum (MHHW). Grid A reflects the modern topography derived from 2009 LiDAR data and includes a straightened outlet channel reconstructed from historical maps and photos (see Figure 2). Grid B depicts the inferred landscape in AD 1700 based on the position of the shoreline in 1925 [*Bernstein*, 1925]. Grid C represents the most landward possible position of the shoreline constrained by a paleo-seacliff buried by sand dunes. Profiles (lower right) along the reconstructed outlet channel compare the modern topography (gray shade) to profiles from alternative model landscapes. Lake outlet elevation in all grids is ~4 m MHHW, equivalent to ~6 m NAVD 88. Grids A–C depict a progressive landward shift of the shoreline, respectively, thereby reducing barriers to tsunami inundation.

positions and tide levels, that successfully simulate inundation in Bradley Lake. The highest slip estimates represent coseismic slip on the megathrust at ~49°N where the plate convergence rate (i.e., slip deficit rate) approaches 40 mm yr^{-1}. Coseismic slip estimates at the latitude of Bradley Lake (43°N) use a convergence rate of 32 mm yr^{-1}. These slip estimates represent the peak values of the slip distributions at the two respective latitudes, including the symmetrical slip, seaward-skewed and splay fault models (Figure 5). Mean slip estimates for the entire rupture area are approximately half the highest slip estimate. It is important to recognize that the peak and mean slip estimates are summary parameters representing the slip distribution of the rupture model used to simulate tsunami inundation. The sixth column in Table 1 lists the time necessary to accrue the corresponding amount of slip at the plate convergence rate, assuming the peak slip recovers all the slip deficit. We stress that sand deposits in the lake only provide lower constraints on inundation capable of exceeding the 6-m lake outlet elevation. Therefore, if prehistoric tsunamis were larger, they would require higher amounts of slip on the megathrust.

5.1. Simulations on a Modern Landscape

[30] Initial experiments simulated tsunami waves that reach Bradley Lake by inundating the modern landscape with a reconstructed, straight outlet channel based on 1925 coastal survey maps (grid A; Figure 6). Westward progradation of the shoreline since 1700 and historical enhancement of foredunes fronting Bradley Lake have placed impediments probably absent when prehistoric tsunamis struck. Using a finite element grid derived from 2009 LiDAR data, simulations required 500–600 year slip deficits to produce tsunamis that reached the 6 m (NAVD 88) elevation of the lake outlet for symmetric and seaward-skewed slip rupture scenarios, respectively. If these models represent full-margin ruptures, they are equivalent to M_w 9–9.1 earthquakes with 16–19 m of slip at 43°N (Table 1). Splay fault scenarios, which emulate greater seafloor uplift (Figure 5), required a 460-year slip deficit accrued at the plate convergence rate (15 m of slip) to simulate tsunami waves that travel up the straightened outlet and into the lake.

[31] Figure 2a shows the simulated tsunami inundation limit for two earthquake scenarios using symmetric slip

Table 1. Cascadia Earthquake Parameters That Simulate Tsunami Inundation in Bradley Lake[a]

Fault Slip Distribution	Length (km)	Width[b] (km)	Slip at 49°N[c] (m)	Slip at 43°N[d] (m)	Mean Slip (m)	Equivalent Years at 40 mm yr^{-1}[e]	Moment Magnitude (M_w)[f]
Modern Shoreline, Straight Outlet Channel (Grid A): MSL + 0.5							
Symmetric slip	1100	105	20	16	10	500	9.0
Seaward-skewed slip[g]	1100	105	24	19	12	600	9.1
Slip diverted to splay fault	1100	83	18	15	9	460	8.9
Inferred 1700 Shoreline (Grid B): MSL + 0.5							
Symmetric slip	1100	105	16	13	8	400	9.0
Slip diverted to splay fault	1100	83	14	12	7	360	8.9
Shoreline Near Seacliff (Grid C): MSL + 0.5							
Symmetric slip	250	55	na	9	6	290	8.4
Slip diverted to splay fault	250	55	na	8	5	260	8.4
Shoreline Near Seacliff (Grid C): MHHW							
Symmetric slip	250	55	na	9	5	270	8.4
Slip diverted to splay fault	250	55	na	8	5	250	8.4

[a]Tidal elevation used in simulations, Mean Sea Level (MSL) + 0.5 m (1.55 m NAVD 88), approximates hindcast tide in 1700 [*Mofjeld et al.*, 1997]. Runs completed with grids A and B use MSL + 0.5 m tide; runs completed with grid C use MSL + 0.5 m and mean higher high water (MHHW, 2.07 m NAVD 88) tides.
[b]Equivalent width for entire fault; actual width at latitude of Bradley Lake is smaller.
[c]Slip estimates are the product of the recurrence interval times a convergence rate close to 40 mm yr^{-1}at ~49°N.
[d]Slip estimates at 43°N use the convergence rate at the latitude of Bradley Lake (32 mm yr^{-1}).
[e]The time, in years, necessary to accrue the corresponding amount of slip at the plate convergence rate.
[f]Moment magnitude (M_w) = (log M_0 − 9.1)/1.5. Seismic moment (M_0), is the product of the rupture area (length × width), mean slip, and rigidity, where rigidity = 4×10^{10} N m^{-2}.
[g]The seaward-skewed slip rupture model was used only for tsunami simulations incorporating grid A.

distributions and a model grid with modern topography. The scenario with a 350-year slip deficit, equivalent to 14 m peak slip, fails to simulate inundation in the lake. A scenario using a 500-year slip deficit, or about 15–16 m of slip, is required to inundate the lake.

[32] The seaward skewed-slip model produced a poorer fit to coseismic subsidence estimates and created smaller tsunamis than the symmetric slip and splay fault models for the same amount of slip (Table 1). Given this finding, we eliminated the seaward-skewed slip model from further testing.

[33] Did past tsunamis face fewer obstacles between the shoreline and the lake than they would today? Historical changes in the landscape present barriers that likely were not faced by prehistoric tsunamis. For example, the introduction of exotic plants in the 1930s to hamper sand dune migration has led to higher foredunes and a seaward shift in the shoreline since 1925 (Figure 2).

5.2. Simulations of the 1700 Tsunami

[34] To test the sensitivity of tsunami simulations to variations in shoreline position and shifting foredunes near the lake outlet we reconstructed plausible landscapes reflecting the inferred shoreline conditions met by prehistoric tsunamis. Of all the tsunami deposits in the lake record, we can reconstruct with most confidence the landscape that existed in 1700. Also available for the 1700 tsunami simulation is the sea level estimate reconstructed by *Mofjeld et al.* [1997]. Although the shoreline conditions in 1700 certainly differed from the present landscape, they probably more closely resembled the coast mapped by early surveyors in the 1920s [*Bernstein*, 1925] before plantings for dune stabilization formed the modern shoreline (Figure 2). Therefore, to estimate the minimum fault slip required by tsunami waves in 1700 that reached Bradley Lake we ran simulations on grid B (Figure 6) using inputs from both the symmetrical slip and splay fault rupture models.

[35] Simulations of the 1700 tsunami require a minimum of 360–400 years of slip (12–13 m peak slip at 43°N) to inundate Bradley Lake for the splay fault and symmetrical slip models, respectively (Table 1). Our findings fall within the range of 10–20 m of slip in 1700 (<550 years of strain accumulation) estimated by *Hawkes et al.* [2011] at Coos Bay using analyses of changes in foraminifera assemblages across stratigraphic contacts attributed to coseismic subsidence. Estimates of slip in 1700 from offshore turbidites at Hydrate Ridge and Rogue Apron are equivocal because *Goldfinger et al.* [2012] could not directly relate turbidite mass to coseismic slip.

5.3. Simulations on a Late Holocene Landscape

[36] Reconstructing the landscape and sea level for earlier Cascadia tsunamis becomes increasingly more difficult for earlier shorelines. Simulations of inferred smaller tsunami waves that inundated the lake about 1,850 and 3,300 cal yr BP (DE6 and DE9 in Figure 4) used grid C that reproduces the most landward position of the late Holocene shoreline revealed by a buried sea cliff (Figure 2). These tests attempt to match waves that deposited thinner tsunami deposits during earlier disturbances in the lake's history when the landscape was likely much different than today's. Overlapping 2σ age ranges (Figure 4) suggest that Cascadia earthquakes recorded by DE6 and DE9 probably represent the same events recorded by turbidites R5a and R7a in Rogue Apron. Although, the DE6 tsunami deposit in Bradley Lake correlates with H5a in Hydrate Ridge, DE9 lacks a correlative turbidite north of Rogue Apron implying that the deposit records a tsunami generated by a Cascadia earthquake restricted to the southern 250 km of the megathrust.

[37] Earthquake scenarios using the splay fault and symmetric slip models with grid C require a minimum of 8–9 m of slip accumulated over 260–290 years, respectively (Table 1), to produce tsunami simulations that inundate Bradley Lake. These simulations used a tide level equivalent to mean sea level plus 0.5 m. Simulations that used a higher tide level (MHHW) required slightly less slip accrued over 250–270 years (Table 1). By reconstructing conditions more favorable for tsunami inundation, we have used paleotsunami deposits in Bradley Lake to estimate the minimum amounts of coseismic slip for inferred earthquakes recorded by thinner, mud turbidites in southern Cascadia. For comparison, *Leonard et al.* [2010] estimated a mean slip of 15 +/− 6 m for pre-1700 earthquakes in southern Oregon (~42.5°–44°N)

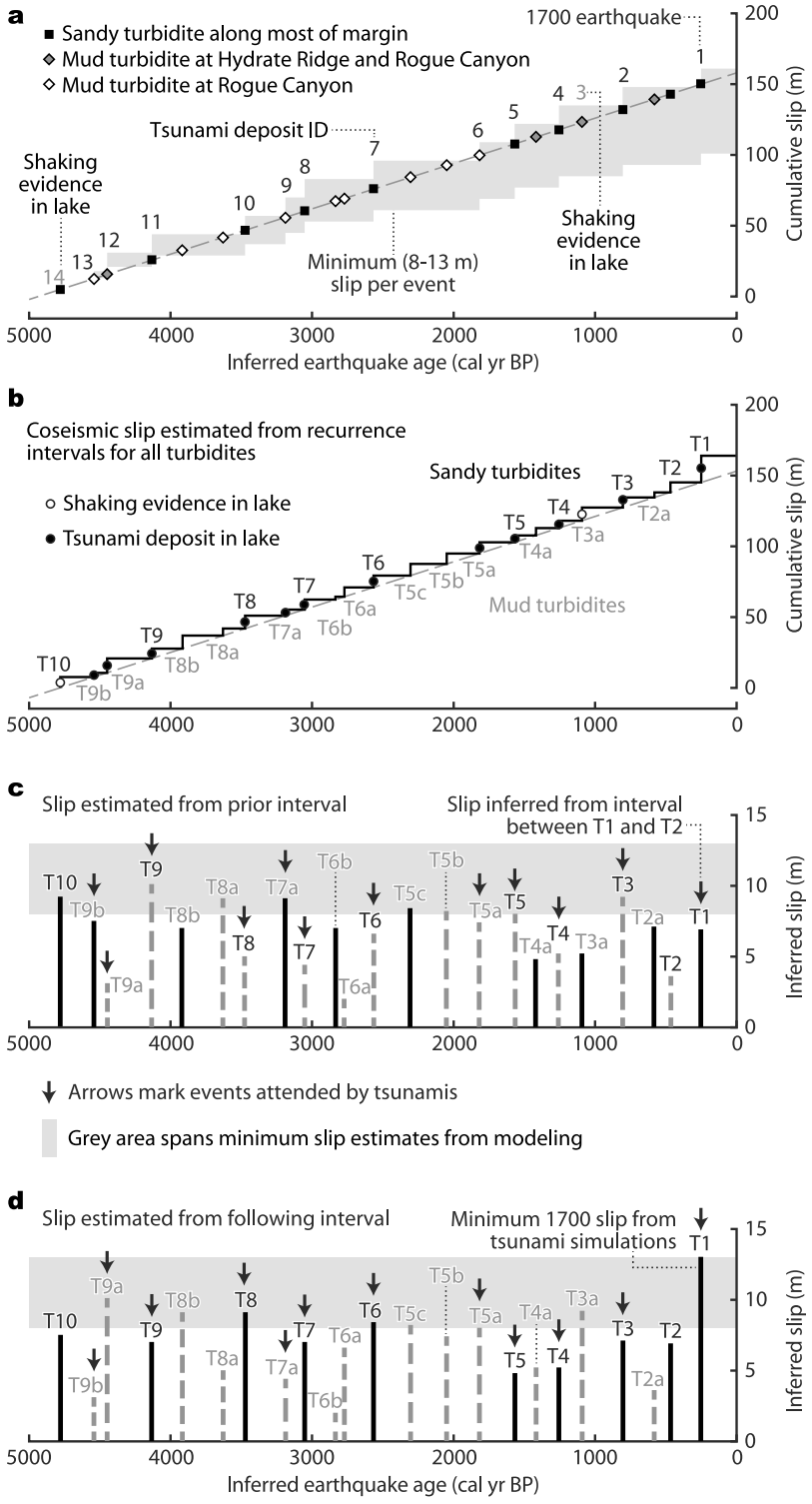

Figure 7

using coseismic subsidence data from the Coquille [*Witter et al.*, 2003] and Sixes Rivers [*Kelsey et al.*, 2002].

5.4. Hypothetical Megathrust Slip Budgets

[38] Hypothetical slip budgets provide insight on the plausibility of estimates constrained by tsunami modeling versus slip deficits implied by paleoseismic recurrence intervals (Figure 7). To construct simple slip budgets, we assume that slip available for fault rupture at the latitude of Bradley Lake accumulates at the convergence rate of ~32 mm yr^{-1} between the Juan de Fuca plate and the Cascadia forearc [*Wang et al.*, 2003] (slope of dashed line in Figure 7a). We also assume that the same part of the megathrust offshore Bradley Lake ruptures during each event. The gray area in the first slip budget (Figure 7a) brackets high and low coseismic slip estimates for each earthquake attended by a tsunami that entered Bradley Lake. The top of this slip envelope uses higher minimum slip estimates constrained by simulations of the 1700 tsunami. If every earthquake accompanied by a tsunami that inundated Bradley Lake involved 12–13 m of slip on the megathrust, then the upper limit of the envelope represents a hypothetical slip budget that leaves little slip available for additional ruptures of the same megathrust patch. Alternatively, if the minimum 8 m of coseismic slip is used for events prior to the 1700 earthquake, this defines the lower boundary of the envelope but leaves approximately 57 m of accumulated slip unspent by earthquakes. If all 11 turbidites that lack correlative tsunami deposits in Bradley Lake reflect rupture of the same megathrust patch, then this 57 m of slip allows a mean slip of ~5.2 m per event, equivalent to 11 M_w 8.2–8.4 earthquakes, magnitude varying with area ruptured.

[39] In contrast, a simple slip budget constructed using turbidite recurrence intervals from the Rogue Apron record is not consistent with coseismic slip estimates from tsunami simulations (Figure 7b). Of the 23 turbidites deposited in Rogue Apron since ~4,600 yr BP, 12 can be reasonably correlated with tsunami deposits in Bradley Lake (Figure 4). Two other turbidites, T3a and T10, appear to correlate with lake disturbances that reflect seismic shaking but lack evidence of tsunami inundation. In Figure 7c, slip is estimated from the inter-event time before a turbidite and compared to the minimum slip estimated from tsunami simulations shown by the horizontal gray band. Arrows point to slip estimates for 12 turbidites that correlate with tsunami deposits, including the 1700 tsunami. Figure 7d shows slip estimates using the post-event time interval between turbidites. Since there hasn't been an earthquake since 1700, there is no post-event interval with which to estimate slip for the most recent Cascadia earthquake. Instead, we use 12–13 m of minimum slip inferred from the 1700 tsunami simulation. Both plots show that among the 11 slip estimates for turbidites that predate 1700, 7 fall short of the minimum slip required to simulate tsunami inundation in Bradley Lake while 4 estimates meet or exceed the minimum slip constraints from modeling.

6. Discussion

[40] Our estimates of coseismic slip on the southern Cascadia megathrust in 1700 suggest the amount of slip may require accumulation over more than one earthquake cycle. A slip deficit of 360–400 years (12–13 m at 32 mm/yr convergence), as indicated by the simulations, is considerably longer than the ~220-year interval between the 1700 earthquake and its predecessor recorded offshore Oregon by turbidite R2 (Figure 4). If turbidite R2a records an earthquake that ruptured the same megathrust slip patch then the slip deficit required by simulations of the 1700 tsunami exceed the slip accrued over two prior earthquake cycles (~330 years, Figure 4). At least in southern Oregon, the interseismic interval preceding the 1700 earthquake appears to be a poor predictor of coseismic slip.

[41] *Leonard et al.* [2010] reported a similar mismatch between the slip in the 1700 earthquake and the prior interval of strain accumulation in southern Washington and northern Oregon. Using a compilation of subsidence data for the 1700 Cascadia earthquake, *Leonard et al.* [2010] estimated slip equivalent to a deficit accumulated over ~500 years along the central Cascadia margin. However, they did not consider the turbidite evidence that the penultimate earthquake was separated by only ~200 years from 1700 along most of the margin [*Goldfinger et al.*, 2012]. Similarly, our results

Figure 7. Hypothetical slip budgets inferred from Bradley Lake tsunami history and offshore turbidite record. (a) Stepwise profile of cumulative slip inferred for 12 Cascadia earthquakes accompanied by tsunamis that inundated Bradley Lake (black numbers). Grey envelope encompasses range of cumulative slip for repeated earthquake cycles with 8–13 m of slip per event. No slip is added for lake disturbances 3 and 14 inferred to record earthquake shaking (gray numbers, Figure 3). Symbols represent turbidites that may or may not correlate with tsunami deposits, including sandy turbidites found along most of the margin (black squares), mud turbidites at Hydrate Ridge and Rogue Apron (gray diamonds), and mud turbidites present only at Rogue Apron (white diamonds). Slope of the dashed line represents the plate convergence rate at the latitude of Bradley Lake (32 mm yr^{-1}). (b) Cumulative earthquake slip profile inferred for turbidite records from Hydrate Ridge and Rogue Apron. Solid line plots cumulative slip for post-event time intervals for all turbidites, including sandy (black labels) and mud turbidites (gray labels) documented in Rogue Apron cores. Black circles mark correlative Cascadia tsunamis evident from sand deposits in Bradley Lake. (c) Coseismic slip inferred from time intervals prior to southern Cascadia turbidites. Bold labels and solid lines show slip estimated for earthquakes recorded by sandy turbidites along most of the margin; gray labels and dashed lines estimate slip from intervals of thinner mud turbidites. Arrows mark turbidites that correlate with tsunami deposits in Bradley Lake. Evidence of seismic shaking in lake sediment may correlate with turbidites T3a and T10. The gray zone spans the minimum fault slip necessary to simulate tsunami inundation in Bradley Lake. Since no earthquake has occurred since turbidite T1, we use the 12–13 m slip estimated from simulating the 1700 tsunami. (d) Coseismic slip inferred from time intervals following southern Cascadia turbidites. Symbols and labels as in Figure 7c. In both Figures 7c and 7d, among the remaining 11 tsunami deposits there are just four cases where turbidite recurrence intervals predict sufficient slip to inundate Bradley Lake that is consistent with tsunami simulations.

conflict with their estimates for the southern part of the subduction zone, which suggest recovered slip deficit accrued over ~200 years, roughly equal to the time between R2 and the 1700 earthquake [*Leonard et al.*, 2010]. *Hawkes et al.* [2011] estimate >10 m of slip in 1700 for the southern Oregon part of the megathrust, which agrees well with our estimates.

[42] *Satake et al.* [2003] estimated 18–21 m peak slip in 1700 (560–660 yrs of slip deficit) based on tsunami wave heights in Japan; however, their coarse, ~400-m numerical grid for tsunami simulations along the Japan coast probably underestimated wave amplitude compared to more refined grids [*Titov and Synolakis*, 1997; *Myers and Baptista*, 2001]. Therefore, the *Satake et al.* [2003] slip estimate on an offshore, full-slip zone spanning the entire length of the megathrust may reflect a maximum slip estimate for the 1700 earthquake.

[43] Working 300 km north of Bradley Lake at Cannon Beach, *Priest et al.* [2009] estimated minimum slip for the last three Cascadia earthquakes at ~14–15 m based on paleotsunami deposits and tsunami simulations similar to this investigation. We conclude that the 1700 Cascadia earthquake had peak slip equal to or exceeding 12–13 m at Bradley Lake and 14–15 m at Cannon Beach, but less than the 18–21 m of *Satake et al.* [2003].

[44] Seismic and tsunami hazard assessments for subduction zones typically rely on earthquake recurrence intervals to estimate fault slip and earthquake magnitude [e.g., *Petersen et al.*, 2008; *González et al.*, 2009]. We question whether the recurrence record of southern Cascadia turbidites alone can be used to reconstruct a reliable slip history of the Cascadia megathrust. Tsunami simulations reported here provide an independent estimate of megathrust slip that meet geological evidence for minimum limits on inundation at Bradley Lake. Our model-constrained slip estimates for southern Cascadia ruptures conflict with lower slip deficits implied by most time intervals between Rogue Apron turbidites (Figure 7) that have been interpreted by *Goldfinger et al.* [2012] to record megathrust earthquakes. A number of explanations could account for the discrepancy: (1) If all southern Cascadia turbidites record great earthquakes on the same megathrust slip patch, then the amount of coseismic slip has varied from one earthquake to the next; (2) thinner mud turbidites may record great earthquakes on patches of the megathrust left unbroken by prior Cascadia earthquakes; or (3) some turbidites may record processes other than rupture of the megathrust (e.g., shallow earthquakes on crustal faults or storms [e.g., *Atwater and Griggs*, 2012], although *Goldfinger et al.* [2012] consider these alternatives unlikely). Discriminating whether or not some of the thinner, mud turbidites reflect sources other than the plate boundary will require closer examination of the offshore record.

[45] If most or all of the turbidites in Rogue Apron record megathrust ruptures, then our results imply that coseismic slip is not simply equal to the slip deficit accumulated since the previous earthquake (e.g., Figure 7). Simple time-predictable or slip-predictable earthquake recurrence models [e.g., *Shimazaki and Nakata*, 1980] founded on the elastic rebound theory [*Reid*, 1910] may be unreliable for the southern Cascadia subduction zone, just as they have been shown to be poor predictors of earthquake size for the southern San Andreas fault [*Weldon et al.*, 2004], the Velino-Magnola fault in Central Italy [*Schlagenhauf et al.*, 2011], the southern Chile megathrust [*Cisternas et al.*, 2005], and now for the Tohoku region of northeastern Japan. For example, paleoseismology of the southern San Andreas fault reveals an earthquake history of long ruptures spanning hundreds of kilometers and sequences of shorter, overlapping ruptures in short time intervals, but no hiatus between earthquakes has lasted longer than ~200 years [*Weldon et al.*, 2005]. In central Italy, earthquake behavior of the Velino-Magnola fault is characterized by long periods of seismic quiescence followed by bursts of slip released during several earthquakes closely spaced in time. *Schlagenhauf et al.* [2011] show how strain that accumulated over a 4–5 ka-long period was released in a cluster of 3 large earthquakes in ~1 ka. And in southern Chile, along the Rio Maullín, *Cisternas et al.* [2005] found evidence of tectonic subsidence and tsunami inundation suggesting that the giant 1960 Chile earthquake (M_w 9.5) released slip stored since its 1575 predecessor of near equal size. In the intervening time, two earthquakes in 1737 and 1837 left few traces of subsidence or tsunamis in estuaries, implying the accumulated strain was not completely released until 1960 [*Cisternas et al.*, 2005]. In these examples, earthquake recurrence intervals fail to provide reliable estimates of slip deficits recovered by fault rupture.

[46] Discrepancies between southern Oregon's onshore and offshore paleoseismological records may reflect variable rupture behavior observed historically at other subduction zones [e.g., *Ando*, 1975; *Kanamori and McNally*, 1982; *Thatcher*, 1990]. Analogues arise in *Schwartz*'s [1999] comparisons of the spatial distribution of moment release for repeat ruptures of the same megathrust segment. Her findings confirm that recurrence behaviors are often more complex than simple characteristic rupture of long-lived asperities. For example, the 1994 northern Honshu and 1995 Solomon Islands earthquakes ruptured areas left unbroken by larger predecessors [*Schwartz*, 1999]. Whereas, the 1995 Kuril Islands and 1996 Aleutian Islands earthquakes ruptured parts of larger asperities involved in earlier larger earthquakes.

[47] Along the Sunda megathrust two earthquakes in 2007 near the Mentawai Islands broke pieces of the giant 1833 rupture zone as revealed by geodetic surveys and coral paleogeodesy revealing a heterogeneous pattern of seismic coupling [*Konca et al.*, 2008]. Sequences of great earthquakes on the Sunda megathrust have been described as supercycles involving large partial failures that culminate in great earthquakes [*Sieh et al.*, 2008].

[48] Offshore Miyagi prefecture, Japan, a history of repeated M 7+ earthquakes was used by *Earthquake Research Committee* [2005] to predict that: "The probability of the occurrence of another similar earthquake in the next 30 years is 99%." However, examinations of original seismograms for several Miyagi-Oki earthquakes in 1933, 1936, 1937, 1978, and 2005 showed that the source regions of the events were too different to justify the probabilistic forecast [*Kanamori et al.*, 2006]. They also pointed out that the series of Miyagi earthquakes accounted for just 1/4 of the plate convergence rate for a part of the megathrust that later broke in the 2011 Tohoku-Oki M_w 9 rupture.

[49] The size of the 2011 Tohoku-Oki earthquake and tsunami exceeded the expectations of many [*Monastersky*, 2011; *Normile*, 2011]. Its magnitude surpassed seismic hazard assessments [*Earthquake Research Committee*, 2005] and model estimates of earthquake size along the Japan

Trench [*Satake et al.*, 2008] checked against written records of tsunamis [*Imamura*, 1934] and tsunami deposits of the past 1500 years [*Sawai et al.*, 2008]. Yet, evidence for the 869 Jogan tsunami, the predecessor of the Tohoku-Oki tsunami, had been known from studies of tsunami deposits for some time [*Abe et al.*, 1990; *Minoura et al.*, 2001]. Variable rupture behavior over successive seismic cycles has been invoked to explain widespread tsunami deposits [*Nanayama et al.*, 2003] and evidence for transient uplift [*Sawai et al.*, 2004] along the coast of the Japanese island of Hokkaido that overlies the Kuril subduction zone.

[50] Lessons from Japan and other convergent margins worldwide suggest that such variability is not exceptional for megathrust earthquakes along subduction zones. Perhaps some sequences of past Cascadia earthquakes have involved ruptures of different patches of the megathrust, which over multiple seismic cycles eventually fill in the seismogenic area like pieces in a jigsaw puzzle. Other earthquakes may have incompletely broken asperities that ruptured during larger predecessors. In light of these possibilities, revisions to Cascadia seismic and tsunami hazard assessments should consider a broader range of rupture scenarios implied by examples at other subduction zones and that are consistent with Cascadia's richly complex paleoseismological record.

7. Remaining Uncertainties

[51] The maximum slip during past earthquakes is unknown and difficult to quantify. Tsunami deposits in Bradley Lake provide only minimum estimates of inundation because sediment transported by wave currents may not extend to the landward limit of runup and post-depositional processes may erode or redeposit tsunami sediment, effectively erasing signs of inundation. Thus, the constraints on megathrust slip provided by tsunami simulations described here are minimum estimates.

[52] The recurrence intervals used here are based on the midpoint of the radiocarbon age range. Earthquake age estimates have considerable 2σ range of uncertainty, including the unquantifiable uncertainty that the radiocarbon data do not match the earthquake age. This uncertainty is discussed but not quantified in most of the original publications we used. *Goldfinger et al.* [2012] attempt to constrain this uncertainty and its component elements. They conclude that based on the statistical tests of fit of multiple ages incorporated in OxCal, tests of accounting for erosion and other errors against control sites, and opportunities for independent checks on the methods that are provided by the 1906 San Andreas and AD 1700 Cascadia earthquakes, that the turbidite ages are unlikely to differ greatly from the earthquake ages. Thus we do not expect that the range of formal uncertainties, and use of the midpoint ages to extract recurrence intervals would be responsible for a systematic bias or non-systematic errors in earthquake ages that would significantly alter our conclusions.

[53] Although we have attempted to reconstruct plausible models of the shoreline and coastal landscape that may have been inundated by past tsunamis, the finite element grids used in the tsunami model are probably very crude representations of the evolving late Holocene coastal landscape at Bradley Lake. In addition, unusual tides or extreme ocean levels may have elevated or lowered some tsunamis.

[54] Like most hydrodynamic computer codes, the two-dimensional, depth-integrated solutions used by the SELFE code to simulate tsunami waves are simplifications of actual tsunami flow dynamics. Furthermore, because the model does not include realistic roughness parameters to account for buildings, vegetation, or other terrain variations, simulations of inundation over dry land may overestimate flooding, and consequently, lead to an underestimation of fault slip. More realistically accounting for the natural roughness of the coastal landscape would likely require higher coseismic slip to simulate tsunami inundation in Bradley Lake.

8. Conclusions

[55] We estimate the minimum amount of megathrust slip necessary to simulate earthquake deformation and tsunami inundation that are compatible with tsunami deposits in Bradley Lake, including evidence for the 1700 Cascadia tsunami and 11 predecessors. Deformation modeling employs three earthquake rupture scenarios: the first partitions slip onto a shallow splay fault; the second distributes slip symmetrically on the megathrust; and the third skews slip seaward. The tsunami simulations use three finite element grids designed to reconstruct (1) the configuration of the coastal landscape and shoreline when the lake outlet was straighter than present, (2) the topography in 1700 when the most recent Cascadia tsunami reached the lake, and (3) conditions during earlier tsunami episodes when the shoreline was probably close to a sea cliff now buried beneath sand dunes. The modeling also considers two tide levels: one consistent with hindcast tidal models estimating the sea level in 1700, and another equal to present mean higher high water. The higher tide level abets a shoreline near the buried sea cliff intended to simulate tsunamis that faced the fewest barriers to lake inundation.

[56] Tsunami simulations provide minimum constraints on the amount of coseismic slip necessary to inundate Bradley Lake considering a range of shoreline positions and three earthquake rupture models. At least 15–19 m of peak slip on the megathrust is necessary to simulate lake inundation using modern topography with a straight lake outlet, equivalent to the release of strain accrued over 500–600 years at the latitude of Bradley Lake. Simulations of the 1700 tsunami consistent with paleoseismological data predict a minimum slip of 12–13 m, equal to a slip deficit accrued over 360–400 years of plate convergence. Minimum coseismic slip during earlier tsunamis facing a shoreline closer to the lake was probably >8–9 m, a slip deficit recovered after periods of 260–290 years. Seafloor deformation produced by Cascadia ruptures with less than 8 m of slip probably produced tsunamis with runups lower than the elevation of the lake outlet.

[57] Along the southern Cascadia subduction zone, deep-sea turbidites from Hydrate Ridge and Rogue Apron have been interpreted to record shaking during great earthquakes on the Cascadia megathrust. Age estimates for the thickest sandy turbidites correlate well with earthquake evidence at many onshore sites, including Bradley Lake. Thinner, mud turbidites are limited to offshore southern Cascadia and occur more frequently than earthquakes inferred from onshore evidence. However, simple coseismic slip budgets derived from turbidite recurrence intervals are inconsistent

with slip estimates constrained by Bradley Lake tsunami deposits. If additional mud turbidites reflect Cascadia ruptures, then the lower bound of the slip budget suggests an average of 5.2 m slip per earthquake at $\sim M_w$ 8.2–8.4, depending on the rupture area. The origin and source of thin, mud turbidites at Rogue Apron that lack reasonable correlatives in Bradley Lake's tsunami record warrant further examination. We propose that some mud turbidites may record ruptures of megathrust patches left unbroken by giant Cascadia subduction zone earthquakes accompanied by tsunamis that inundated Bradley Lake, or they released stored energy from previous seismic cycles. If all mud turbidites at Hydrate Ridge and Rogue Apron reflect ruptures of the underlying plate boundary, then their recurrence intervals are poor predictors of coseismic slip because only one-third of the intervals between turbidites imply coseismic slip consistent with tsunami simulations.

[58] In summary, new constraints on coseismic slip obtained from tsunami simulations constrained by geological observations of tsunami inundation suggest considerable heterogeneity in temporal and spatial rupture behavior of the southern Cascadia megathrust. Such heterogeneity in Cascadia, and that observed in other subduction settings, stress the importance of using paleoseismological data in future revisions of seismic and tsunami hazard assessments in Cascadia and elsewhere.

[59] **Acknowledgments.** A grant from NOAA's National Tsunami Hazard Mitigation Program (grant NA08NWS4670028) provided partial funding for this project. Reviews by B. Atwater, J. N. Proust, A. Sladen, and R. Wells prompted expansion of the paper, refocused the discussion, and led to many improvements. Discussions with H. Kelsey, A. Nelson, and J. Witter helped clarify the ideas presented here. Author responsibilities: R.W., K.W., C.G. and G.P. developed the earthquake scenarios. K.W. modeled fault dislocation to simulate earthquake deformation. Y.Z. performed tsunami modeling. J.A. performed storm wave runup modeling. R.W. prepared the manuscript and illustrations. This research is a contribution toward National Science Foundation award EAR-0842728 and IGCP 588 coastal change.

References

Abe, H., Y. Sugeno, and A. Chigama (1990), Estimation of the height of the Sanriku Jogan 11 earthquake-tsunami (A.D. 869) in the Sendai Plain, *Zisin*, *43*, 513–525.

Adams, J. (1990), Paleoseismicity of the Cascadia subduction zone: Evidence from turbidites off the Oregon-Washington margin, *Tectonics*, *9*, 569–583, doi:10.1029/TC009i004p00569.

Ando, M. (1975), Source mechanisms and tectonic significance of historical earthquakes along the Nankai Trough, Japan, *Tectonophysics*, *27*, 119–140, doi:10.1016/0040-1951(75)90102-X.

Atwater, B. F., and G. B. Griggs (2012), Deep-Sea turbidites as guides to Holocene earthquake history at the Cascadia Subduction Zone—Alternative views for a seismic-hazard workshop, *U.S. Geol. Surv. Open File Rep.*, *2012–1043*, 58 pp.

Atwater, B. F., and E. Hemphill-Haley (1997), Recurrence intervals for great earthquakes of the past 3500 years at northeastern Willapa Bay, Washington, *U.S. Geol. Surv. Prof. Pap.*, *1576*, 108 pp.

Bernstein, E. H. (1925), Topography of the Oregon coast south of Coquille River, *T-Sheet 4216*, 1:20,000 scale, U.S. Natl. Geod. Surv., Silver Spring, Md.

Briggs, R. W., et al. (2006), Deformation and slip along the Sunda megathrust in the great 2005 Nias-Simeulue earthquake, *Science*, *311*, 1897–1901, doi:10.1126/science.1122602.

Cisternas, M., et al. (2005), Predecessors of the giant 1960 Chile earthquake, *Nature*, *437*, 404–407, doi:10.1038/nature03943.

Clarke, S. H., and G. A. Carver (1992), Late Holocene tectonics and paleoseismicity, southern Cascadia subduction zone, *Science*, *255*(5041), 188–192, doi:10.1126/science.255.5041.188.

DeMets, C., R. G. Gordon, and D. F. Argus (2010), Geologically current plate motions, *Geophys. J. Int.*, *181*, 1–80, doi:10.1111/j.1365-246X.2009.04491.x.

Earthquake Research Committee (2005), National seismic hazard maps for Japan, report, Headquarters for Earthquake Res. Promot., Tokyo. [Available at http://www.jishin.go.jp/main/index-e.html]

Frankel, A. (2011), Summary of meeting to evaluate Cascadia turbidite data for the National Seismic Hazard Maps, *U.S. Geol. Surv. Open File Rep.*, *2011-1310*, 13 pp.

Freund, L. B., and D. M. Barnett (1976), A two-dimensional analysis of surface deformation due to dip-slip faulting, *Bull. Seismol. Soc. Am.*, *66*, 667–675.

Fujiwara, T., S. Kodaira, T. No, Y. Kaiho, N. Takahashi, and Y. Kaneda (2011), The 2011 Tohoku-Oki earthquake: Displacement reaching the trench axis, *Science*, *334*(6060), 1240.

Goldfinger, C., et al. (2008), Late Holocene rupture of the northern San Andreas Fault and possible stress linkage to the Cascadia Subduction Zone, *Bull. Seismol. Soc. Am.*, *98*, 861–889, doi:10.1785/0120060411.

Goldfinger, C., et al. (2012), Turbidite event history: Methods and implications for Holocene paleoseismicity of the Cascadia Subduction Zone, *U.S. Geol. Surv. Prof. Pap.*, *1661-F*, 184 pp.

González, F. I., et al. (2009), Probabilistic tsunami hazard assessment at Seaside, Oregon, for near- and far-field seismic sources, *J. Geophys. Res.*, *114*, C11023, doi:10.1029/2008JC005132.

Gorsline, D. S., T. De Diego, and E. H. Nava-Sanchez (2000), Seismically triggered turbidites in small margin basins: Alfonso Basin, western Gulf of California and Santa Monica Basin, California borderland, *Sediment. Geol.*, *135*, 21–35, doi:10.1016/S0037-0738(00)00060-9.

Gràcia E., A. Vizcaino, C. Escutia, A. Asioli, A. Rodés, R. Pallàs, J. Garcia-Orellana, S. Lebreiro, and C. Goldfinger (2010), Holocene earthquake record offshore Portugal (SW Iberia): Applying turbidite paleoseismology in a slow-convergence margin, *Quat. Sci. Rev.*, *29*, 1156–1172, doi:10.1016/j.quascirev.2010.01.010.

Griggs, G. B., and L. D. Kulm (1970), Sedimentation in Cascadia deep-sea channel, *Geol. Soc. Am. Bull.*, *81*, 1361–1384, doi:10.1130/0016-7606(1970)81[1361:SICDC]2.0.CO;2.

Hawkes, A. D., B. P. Horton, A. R. Nelson, C. H. Vane, and Y. Sawai (2011), Coastal subsidence in Oregon, USA, during the giant Cascadia earthquake of AD 1700, *Quat. Sci. Rev.*, *30*, 364–376, doi:10.1016/j.quascirev.2010.11.017.

Hughen, K. A., et al. (2004), Marine04 marine radiocarbon age calibration, 26–0 ka BP, *Radiocarbon*, *46*, 1059–1086.

Ide, S., A. Baltay, and G. C. Beroza (2011), Shallow dynamic overshoot and energetic deep rupture in the 2011 Mw 9.0 Tohoku-Oki earthquake, *Science*, *332*, 1426–1429, doi:10.1126/science.1207020.

Imamura, A. (1934), Past tsunamis of the Sanriku coast, *Jpn. J. Astron. Geophys.*, *11*, 79–93.

Kanamori, H., and K. C. McNally (1982), Variable rupture mode of the subduction zone along the Ecuador-Colombia coast, *Bull. Seismol. Soc. Am.*, *72*, 1241–1253.

Kanamori, H., M. Miyazawa, and J. Mori (2006), Investigation of the earthquake sequence off Miyagi prefecture with historical seismograms, *Earth Planets Space*, *58*, 1533–1541.

Kelsey, H. M., R. C. Witter, and E. Hemphill-Haley (2002), Plate-boundary earthquakes and tsunamis of the past 5,500 yr, Sixes River estuary, southern Oregon, *Geol. Soc. Am. Bull.*, *114*, 298–314, doi:10.1130/0016-7606(2002)114<0298:PBEATO>2.0.CO;2.

Kelsey, H. M., A. R. Nelson, E. Hemphill-Haley, and R. C. Witter (2005), Tsunami history of an Oregon coastal lake reveals a 4600 yr record of great earthquakes on the Cascadia subduction zone, *Geol. Soc. Am. Bull.*, *117*(7), 1009–1032, doi:10.1130/B25452.1.

Komar, P. (1997), *The Pacific Northwest Coast: Living With the Shores of Oregon and Washington*, Duke Univ. Press, Durham, N. C.

Komar, P. D., J. C. Allan, and P. Ruggiero (2011), Sea level variations along the U.S. Pacific Northwest coast: Tectonic and climate controls, *J. Coastal Res.*, *27*, 808–823, doi:10.2112/JCOASTRES-D-10-00116.1.

Konca, A. O., et al. (2008), Partial rupture of a locked patch of the Sumatra megathrust during the 2007 earthquake sequence, *Nature*, *456*, 631–635, doi:10.1038/nature07572.

Leonard, L. J., R. D. Hyndman, and S. Mazzotti (2004), Coseismic subsidence in the 1700 Great Cascadia earthquake: Coastal estimates versus elastic dislocation models, *Geol. Soc. Am. Bull.*, *116*, 655–670, doi:10.1130/B25369.1.

Leonard, L. J., C. A. Currie, S. Mazzotti, and R. D. Hyndman (2010), Rupture area and displacement of past Cascadia great earthquakes from coastal coseismic subsidence, *Geol. Soc. Am. Bull.*, *122*(11–12), 1951–1968, doi:10.1130/B30108.1.

MacInnes, B. T., R. Weiss, J. Bourgeois, and T. K. Pinegina (2010), Slip distribution of the 1952 Kamchatka great earthquake based on near-field tsunami deposits and historical records, *Bull. Seismol. Soc. Am.*, *100*(4), 1695–1709, doi:10.1785/0120090376.

McCalpin, J. P., and A. R. Nelson (1996), Introduction to paleoseismology, in *Paleoseismology*, edited by J. P. McCalpin, pp. 1–32, Academic, Orlando, Fla., doi:10.1016/S0074-6142(96)80068-4.

Meyers, R. A., D. G. Smith, H. M. Jol, and C. D. Peterson (1996), Evidence for eight great earthquake-subsidence events detected with ground-penetrating radar, Willapa barrier, Washington, *Geology*, *24*, 99–102, doi:10.1130/0091-7613(1996)024<0099:EFEGES>2.3.CO;2.

Minoura, K., F. Imamura, D. Sugawara, Y. Kono, and T. Iwashita (2001), The 869 Jogan tsunami deposit and recurrence interval of large-scale tsunami on the Pacific coast of northeast Japan, *J. Nat. Disaster Sci.*, *23*, 83–88.

Mofjeld, H. O., M. G. G. Foreman, and A. Ruffman (1997), West Coast tides during Cascadia subduction zone tsunamis, *Geophys. Res. Lett.*, *24*(17), 2215–2218, doi:10.1029/97GL02060.

Monastersky, R. (2011), Giant shock rattles ideas about quake behavior, *Nature*, *471*, 274, doi:10.1038/471274a.

Myers, E. P., and A. M. Baptista (2001), Analysis of factors influencing simulations of the1993 Hokkaido Nansei-Oki and 1964 Alaska tsunamis, *Nat. Hazards*, *23*, 1–28, doi:10.1023/A:1008150210289.

Nakajima, T., and Y. Kanai (2000), Sedimentary features of seismoturbidites triggered by the 1983 and older historical earthquakes in the eastern margin of the Japan Sea, *Sediment. Geol.*, *135*, 1–19, doi:10.1016/S0037-0738(00)00059-2.

Nanayama, F., K. Satake, R. Furukawa, K. Shimokawa, B. F. Atwater, K. Shigeno, and S. Yamaki (2003), Unusually large earthquakes inferred from tsunami deposits along the Kuril Trench, *Nature*, *424*, 660–663, doi:10.1038/nature01864.

Nelson, A. R. (1992), Holocene tidal-marsh stratigraphy in south-central Oregon—Evidence for localized sudden submergence in the Cascadia subduction zone, in *Quaternary Coasts of the United States: Lacustrine and Marine Systems*, edited by C. P. Fletcher and J. F. Wehmiller, *Spec. Publ. SEPM Soc. Sediment. Geol.*, *48*, 287–301, doi:10.2110/pec.92.48.0287.

Nelson, A. R., A. E. Jennings, and K. Kashima (1996), An earthquake history derived from stratigraphic and microfossil evidence of relative sea-level change at Coos Bay, southern coastal Oregon, *Geol. Soc. Am. Bull.*, *108*, 141–154, doi:10.1130/0016-7606(1996)108<0141:AEHDFS>2.3.CO;2.

Nelson, A. R., Y. Ota, M. Umitsu, K. Kashima, and Y. Matshushima (1998), Seismic or hydrodynamic control of rapid late-Holocene sea-level rise in southern coastal Oregon, USA?, *Holocene*, *8*, 287–299, doi:10.1191/095968398668600476.

Nelson, A. R., H. M. Kelsey, and R. C. Witter (2006), Great earthquakes of variable magnitude at the Cascadia subduction zone, *Quat. Res.*, *65*, 354–365, doi:10.1016/j.yqres.2006.02.009.

Nelson, A. R., Y. Sawai, A. E. Jennings, L.-A. Bradley, L. Gerson, B. L. Sherrod, J. Sabean, and B. P. Horton (2008), Great-earthquake paleogeodesy and tsunamis of the past 2000 years at Alsea Bay, central Oregon coast, USA, *Quat. Sci. Rev.*, *27*(7–8), 747–768, doi:10.1016/j.quascirev.2008.01.001.

Normile, D. (2011), Devastating earthquake defied expectations, *Science*, *331*, 1375–1376, doi:10.1126/science.331.6023.1375.

Okada, Y. (1985), Surface deformation due to shear and tensile faults in a half-space, *Bull. Seismol. Soc. Am.*, *75*(4), 1135–1154.

Petersen, M. D., et al. (2008), Documentation for the 2008 update of the United States National Seismic Hazard Maps, *U.S. Geol. Surv. Open File Rep.*, *1128*, 61 pp.

Pilkey, O. H. (1988), Basin Plains: Giant sedimentation events, *Spec. Pap. Geol. Soc. Am.*, *229*, 93–99.

Priest, G. R., C. Goldfinger, K. Wang, R. C. Witter, Y. Zhang, and A. M. Baptista (2009), Confidence levels for tsunami-inundation limits in northern Oregon inferred from a 10,000-year history of great earthquakes at the Cascadia subduction zone, *Nat. Hazards*, *54*, 27–73, doi:10.1007/s11069-009-9453-5.

Reid, H. F. (1910), The mechanics of the earthquake, in *The California Earthquake of April 18, 1906: Report of the State Earthquake Investigation Commission*, vol. 2, pp. 16–28, Carnegie Inst. of Wash., Washington, D. C.

Reimer, P. J., et al. (2004), IntCal04 terrestrial radiocarbon age calibration, 26–0 ka BP, *Radiocarbon*, *46*, 1029–1058.

Satake, K., K. Shimazaki, Y. Tsuji, and K. Ueda (1996), Time and size of a giant earthquake in Cascadia inferred from Japanese tsunami records of January 1700, *Nature*, *379*, 246–249, doi:10.1038/379246a0.

Satake, K., K. Wang, and B. F. Atwater (2003), Fault slip and seismic moment of the 1700 Cascadia earthquake inferred from Japanese tsunami descriptions, *J. Geophys. Res.*, *108*(B11), 2535, doi:10.1029/2003JB002521.

Satake, K., Y. Namegaya, and S. Yamaki (2008), Numerical simulation of the AD 869 Jogan tsunami in Ishinomaki and Sendai plains, *Annu. Rep. Active Fault Paleoearthquake Res., 8*, pp. 71–89, Active Fault and Earthquake Res. Cent., Tsukuba, Japan.

Sawai, Y., K. Satake, T. Kamataki, H. Nasu, M. Shishikura, B. F. Atwater, B. P. Horton, H. M. Kelsey, T. Nagumo, and M. Yamaguchi (2004), Transient uplift after a 17th-century earthquake along the Kuril subduction zone, *Science*, *306*, 1918–1920, doi:10.1126/science.1104895.

Sawai, Y., Y. Fujii, O. Fujiwara, T. Kamataki, J. Komatsubara, Y. Okamura, K. Satake, and M. Shishikura (2008), Marine incursions of the past 1500 years and evidence of tsunamis at Suijin-numa, a coastal lake facing the Japan Trench, *Holocene*, *18*(4), 517–528, doi:10.1177/0959683608089206.

Schlagenhauf, A., I. Manighetti, L. Benedetti, Y. Gaudemer, R. Finkel, J. Malavieille, and K. Pou (2011), Earthquake supercycles in central Italy, inferred from ^{36}Cl exposure dating, *Earth Planet. Sci. Lett.*, *307*, 487–500, doi:10.1016/j.epsl.2011.05.022.

Schwartz, S. (1999), Noncharacteristic behavior and complex recurrence of large subduction zone earthquakes, *J. Geophys. Res.*, *104*, 23,111–23,125, doi:10.1029/1999JB900226.

Shimazaki, K., and T. Nakata (1980), Time-predictable recurrence model for large earthquakes, *Geophys. Res. Lett.*, *7*, 279–282, doi:10.1029/GL007i004p00279.

Sieh, K., et al. (2008), Earthquake supercyles inferred from sea-level changes recorded in the corals of West Sumatra, *Science*, *322*, 1674–1678, doi:10.1126/science.1163589.

Stuiver, M., and P. J. Reimer (1993), Extended ^{14}C data base and revised CALIB 3.0 ^{14}C age calibration programme, *Radiocarbon*, *35*(1), 215–231.

Thatcher, W. (1990), Order and diversity in the modes of circum-Pacific earthquake recurrence, *J. Geophys. Res.*, *95*(B3), 2609–2623, doi:10.1029/JB095iB03p02609.

Titov, V. V., and C. E. Synolakis (1997), Extreme inundation flows during the Hokkaido-Nansei-Oki tsunami, *Geophys. Res. Lett.*, *24*(11), 1315–1318, doi:10.1029/97GL01128.

Titov, V. V., B. E. Jaffe, F. I. González, and G. Gelfenbaum (2001), Re-evaluating source mechanisms for the 1998 Papua New Guinea tsunami using revised slump estimates and sedimentation modeling, in *Proceedings of the International Tsunami Symposium*, vol. 2, pp. 389–396, NOAA, Seattle, Wash. [Available at http://nthmp-history.pmel.noaa.gov/its2001/]

Wang, K., and J. He (2008), Effects of frictional behaviour and geometry of subduction fault on coseismic seafloor deformation, *Bull. Seismol. Soc. Am.*, *98*(2), 571–579, doi:10.1785/0120070097.

Wang, K., and Y. Hu (2006), Accretionary prisms in subduction earthquake cycles: The theory of dynamic Coulomb wedge, *J. Geophys. Res.*, *111*, B06410, doi:10.1029/2005JB004094.

Wang, K., R. Wells, S. Mazzotti, R. D. Hyndman, and T. A. Sagiya (2003), Revised dislocation model of interseismic deformation of the Cascadia subduction zone, *J. Geophys. Res.*, *108*(B1), 2026, doi:10.1029/2001JB001227.

Weldon, R., K. Scharer, T. Fumal, and G. Biasi (2004), Wrightwood and the earthquake cycle: What a long recurrence record tells us about how faults work, *GSA Today*, *14*(9), 4–10, doi:10.1130/1052-5173(2004)014<4:WATECW>2.0.CO;2.

Weldon, R., T. Fumal, G. Biasi, and K. Scharer (2005), Past and future earthquakes on the San Andreas fault, *Science*, *308*, 966–967, doi:10.1126/science.1111707.

Witter, R. C., H. M. Kelsey, and E. Hemphill-Haley (2003), Great Cascadia earthquakes and tsunamis of the past 6700 years, Coquille River estuary, southern coastal Oregon, *Geol. Soc. Am. Bull.*, *115*, 1289–1306, doi:10.1130/B25189.1.

Zhang, Y., and A. M. Baptista (2008), An efficient and robust tsunami model on unstructured grids. Part I: Inundation benchmarks, *Pure Appl. Geophys.*, *165*(11–12), 2229–2248, doi:10.1007/s00024-008-0424-7.

Zhang, Y., R. C. Witter, and G. R. Priest (2011), Tsunami–tide interaction in 1964 Prince William Sound tsunami, *Ocean Modell.*, *40*, 246–259, doi:10.1016/j.ocemod.2011.09.005.